NLO Higgs boson production via gluon fusion matched with shower in POWHEG

JHEP04(2009)002

(http://iopscience.iop.org/1126-6708/2009/04/002)

Published by IOP Publishing for SISSA

Received: *January 15, 2009*
Revised: *February 12, 2009*
Accepted: *March 6, 2009*
Published: *April 1, 2009*

JHEP04(2009)002

NLO Higgs boson production via gluon fusion matched with shower in POWHEG

Simone Alioli,[a,b] **Paolo Nason,**[b] **Carlo Oleari**[a,b] **and Emanuele Re**[a,b]

[a] *Università di Milano-Bicocca, Sezione di Milano-Bicocca, Piazza della Scienza 3, 20126 Milan, Italy*
[b] *INFN, Sezione di Milano-Bicocca, Piazza della Scienza 3, 20126 Milan, Italy*
E-mail: Simone.Alioli@mib.infn.it, Paolo.Nason@mib.infn.it, Carlo.Oleari@mib.infn.it, Emanuele.Re@mib.infn.it

Abstract: We present a next-to-leading order calculation of Higgs boson production via gluon fusion interfaced to shower Monte Carlo programs, implemented according to the POWHEG method. A detailed comparison with MC@NLO and PYTHIA is carried out for several observables, for the Tevatron and LHC colliders. Comparisons with next-to-next-to-leading order results and with resummed ones are also presented.

Keywords: NLO Computations, QCD,Hadronic Colliders

doi:10.1088/1126-6708/2009/04/002

Contents

JHEP04(2009)002

1 Introduction

Gluon fusion is the dominant Higgs boson production mechanism both at the Tevatron and at the LHC. Radiative corrections to this process are known to be large [1–3], and it is thus important that shower generators that do include them are made available to the experimental collaborations. In fact, one such generator already exists, namely the MC@NLO implementation [4] of Higgs boson production.

In this work we present a next-to-leading order (NLO) calculation of Higgs boson production via gluon fusion, interfaced to shower Monte Carlo programs according to the POWHEG method. Unlike the MC@NLO implementation, our generator produces events with positive (constant) weight, and, furthermore, is not tied to the HERWIG shower Monte Carlo

program. It can be easily interfaced to any modern shower generator and, in fact, we show results of POWHEG interfaced to HERWIG [5, 6] and to PYTHIA [7].

The POWHEG method was first suggested in ref. [8]. In ref. [9] a detailed general description of its application to collider processes was given. Until now, the POWHEG method has been applied to ZZ pair hadroproduction [10], heavy-flavour production [11], e^+e^- annihilation into hadrons [12] and into top pairs [13], and Drell-Yan vector boson production [14, 15]. We have built our implementation of the Higgs boson production by following closely the formulae and results of ref. [9].

Much of our phenomenological section will be devoted to study the comparison of our result with that of MC@NLO. We find fair agreement between MC@NLO and POWHEG results, except for the p_{T} distribution of the Higgs boson, and consequently of the hardest jet, in the high-p_{T} region. In this region, the POWHEG distributions are generally harder. We have shown that this is due to next-to-next-to-leading order (NNLO) effects in the POWHEG formula for the differential cross section. We checked that these effects actually bring our result closer to the NNLO one [16]. Other relevant discrepancies are found in the rapidity difference of the Higgs boson and the hardest jet. The dip produced by the MC@NLO program, found in previous implementations [10, 11, 14], is present also here. We remark that this seems to be a general feature of MC@NLO, since other calculations do not find effects of this kind [17–19].

The paper is organized as follows. In section 2 we describe how we performed the calculation for the Higgs boson cross section at the next-to-leading order. In section 3 we discuss the POWHEG implementation. In section 4 we show our results for several kinematic variables and compare them with the MC@NLO [4] and PYTHIA 6.4 [7] shower Monte Carlo programs. A comparison with next-to-next-to-leading order results, as well as with analytical resummed ones is also carried out. In section 5, we give our conclusions.

2 Description of the calculation

In this section we fix our kinematic notation, and give the Higgs boson production differential cross sections up to next-to-leading order in the strong coupling α_{S}.

2.1 Kinematics

2.1.1 Born kinematics

The Born process has a single partonic contribution, $gg \to H$. Following the notation of ref. [9], we denote with $\bar{k}_{\oplus}$ and $\bar{k}_{\ominus}$ the incoming gluon momenta, aligned along the plus and minus direction of the z axis, and by $\bar{k}_1$ the outgoing Higgs boson momentum. If $K_{\oplus}$ and $K_{\ominus}$ are the momenta of the incoming hadrons, then we have

$$\bar{k}_{\circledast} = \bar{x}_{\circledast} K_{\circledast} \,, \tag{2.1}$$

where $\bar{x}_{\circledast}$ are the momentum fractions, and momentum conservation reads

$$\bar{k}_{\oplus} + \bar{k}_{\ominus} = \bar{k}_1 \,. \tag{2.2}$$

JHEP04(2009)002

We introduce the Higgs boson invariant mass squared and rapidity

$$M^2 = \bar{k}_1^2, \qquad Y = \frac{1}{2}\log\frac{\bar{k}_1^0 + \bar{k}_1^3}{\bar{k}_1^0 - \bar{k}_1^3}\,, \tag{2.3}$$

so that the set of variables $\bar{\mathbf{\Phi}}_1 \equiv \left\{M^2, Y\right\}$ fully parametrizes the Born kinematics. From them, we can reconstruct the momentum fractions

$$\bar{x}_\oplus = \sqrt{\frac{M^2}{S}}e^{Y}, \qquad \bar{x}_\ominus = \sqrt{\frac{M^2}{S}}e^{-Y}, \tag{2.4}$$

where $S = (K_\oplus + K_\ominus)^2$ is the squared center-of-mass energy of the hadronic collider. The Born phase space, in terms of these variables, can be written as

$$d\bar{\mathbf{\Phi}}_1 = d\bar{x}_\oplus\, d\bar{x}_\ominus (2\pi)^4 \delta^4\left(\bar{k}_\oplus + \bar{k}_\ominus - \bar{k}_1\right)\frac{d^3\bar{k}_1}{(2\pi)^3 2\bar{k}_1^0} = \frac{2\pi}{S}\delta\big(M^2 - m_H^2\big)\, dM^2\, dY\,. \tag{2.5}$$

We generate the Higgs boson virtuality according to a Breit-Wigner distribution, i.e. we make the replacement[1]

$$\delta\big(M^2 - m_H^2\big) \;\to\; \frac{1}{\pi}\frac{M^2\,\Gamma_H/m_H}{\big(M^2 - m_H^2\big)^2 + (M^2\,\Gamma_H/m_H)^2}. \tag{2.6}$$

The decay of the Higgs boson is left to the shower Monte Carlo program, since, being the Higgs boson a scalar, no spin correlation can arise.

2.1.2 Real-emission kinematics

The real emission processes have an additional final-state parton, so that momentum conservation reads

$$k_\oplus + k_\ominus = k_1 + k_2\,, \tag{2.7}$$

where k_1 is the Higgs boson momentum and k_2 is the momentum of the additional final-state parton in the laboratory frame and

$$k_{\textcircled{a}} = x_{\textcircled{a}} K_{\textcircled{a}}\,. \tag{2.8}$$

Since we regularize the infrared divergences in the Frixione, Kunszt and Signer (FKS) subtraction scheme [20, 21], we introduce the appropriate set of radiation variables. In the partonic center-of-mass frame, the final-state parton has momentum

$$k_2' = k_2'^0\ (1, \sin\theta\sin\phi, \sin\theta\cos\phi, \cos\theta), \tag{2.9}$$

and we use the set $\Phi_{\rm rad} \equiv \{\xi, y, \phi\}$ as radiation variables, where

$$k_2'^0 = \frac{\sqrt{s}}{2}\xi, \qquad y = \cos\theta\,, \tag{2.10}$$

[1] In order to compare our result with other programs, we have also used slightly different forms of the Breit-Wigner distribution, that will be illustrated in due time.

JHEP04(2009)002

and

$$s = (k_\oplus + k_\ominus)^2 = \frac{M^2}{1-\xi} \tag{2.11}$$

is the partonic center-of-mass energy squared. Since there are no final-state coloured partons at the Born level, we have to deal with initial-state singularities only. The soft singularity is characterized by $\xi \to 0$, while the collinear limits (k_2 parallel to the $\oplus$ or $\ominus$ incoming directions) are characterized by $y \to 1$ and $y \to -1$ respectively.

2.1.3 Inverse construction

The set of variables $\mathbf{\Phi}_2 \equiv \{M^2, Y, \xi, y, \phi\}$ fully specifies the real-emission kinematics. In fact, given these variables, we can reconstruct all the momenta. Using eq. (2.4), we can compute the underlying Born momentum fractions $\bar{x}_{\oplus}$ and, following section 5 of ref [9], we have

$$x_\oplus = \frac{\bar{x}_\oplus}{\sqrt{1-\xi}}\sqrt{\frac{2-\xi(1-y)}{2-\xi(1+y)}}, \qquad x_\ominus = \frac{\bar{x}_\ominus}{\sqrt{1-\xi}}\sqrt{\frac{2-\xi(1+y)}{2-\xi(1-y)}}, \tag{2.12}$$

with the kinematics constraints

$$0 \le \xi \le \xi_{\rm M}(y)\,, \tag{2.13}$$

where

$$\xi_{\rm M}(y) = 1 - \max\left\{ \frac{2(1+y)\,\bar{x}_\oplus^2}{\sqrt{(1+\bar{x}_\oplus^2)^2(1-y)^2 + 16\,y\,\bar{x}_\oplus^2} + (1-y)(1-\bar{x}_\oplus^2)}, \right.$$
$$\left. \frac{2(1-y)\,\bar{x}_\ominus^2}{\sqrt{(1+\bar{x}_\ominus^2)^2(1+y)^2 - 16\,y\,\bar{x}_\ominus^2} + (1+y)(1-\bar{x}_\ominus^2)} \right\}. \tag{2.14}$$

The momentum of the final-state parton in the partonic center-of-mass frame is given by eqs. (2.9) and (2.10). We then make a longitudinal boost $\mathbb{B}_L$ from the center-of-mass frame back to the laboratory frame, with boost velocity

$$\beta = \frac{x_\oplus - x_\ominus}{x_\oplus + x_\ominus}\,, \tag{2.15}$$

to obtain k_2 from k_2'

$$k_2 = \mathbb{B}_L\, k_2'\,. \tag{2.16}$$

From momentum conservation, we reconstruct the Higgs boson momentum

$$k_1 = x_\oplus K_\oplus + x_\ominus K_\ominus - k_2\,. \tag{2.17}$$

Finally, the two-body phase space can be written in a factorized form in terms of the Born and radiation phase space

$$d\mathbf{\Phi}_2 = dx_\oplus\, dx_\ominus (2\pi)^4 \delta^4(k_\oplus + k_\ominus - k_1 - k_2) \frac{d^3k_1}{(2\pi)^3 2k_1^0} \frac{d^3k_2}{(2\pi)^3 2k_2^0} = d\bar{\mathbf{\Phi}}_1\, d\Phi_{\rm rad}\,, \tag{2.18}$$

where

$$d\Phi_{\rm rad} = \frac{M^2}{(4\pi)^3} \frac{\xi}{(1-\xi)^2}\, d\xi\, dy\, d\phi\,. \tag{2.19}$$

JHEP04(2009)002

2.2 Cross sections

In order to apply the POWHEG method, we need the Born, real and virtual contributions to the differential cross section, i.e. the squared amplitudes, averaged over colours and helicities of the incoming partons, and multiplied by the appropriate flux factor.

2.2.1 Born contribution

At Born level, Higgs boson production via gluon fusion proceeds through the coupling of the Higgs boson to a heavy-quark loop. The squared matrix element for the lowest-order contribution, averaged over colours and helicities of the incoming gluons, and multiplied by the flux factor $1/(2M^2)$, is given by

$$\mathcal{B}_{gg} = \frac{\alpha_{\rm S}^2}{\pi^2}\frac{G_F\, M^2}{576\sqrt{2}}\left|\frac{3}{2}\sum_Q \tau_Q\Big[1+(1-\tau_Q)f(\tau_Q)\Big]\right|^2, \tag{2.20}$$

where $\tau_Q = 4m_Q^2/M^2$, and the sum runs over the heavy flavours with mass m_Q circulating in the loop. The function f is given by

$$f(\tau_Q) = \begin{cases} \arcsin^2\dfrac{1}{\sqrt{\tau_Q}} & \tau_Q \geq 1\,, \\ -\dfrac{1}{4}\left[\log\left(\dfrac{1+\sqrt{(1-\tau_Q)}}{1-\sqrt{(1-\tau_Q)}}\right) - i\pi\right]^2 & \tau_Q < 1. \end{cases} \tag{2.21}$$

In our implementation we only retain the contribution coming from the top quark.

2.2.2 Virtual corrections

In the calculation of all NLO corrections, we have used an effective Lagrangian, where the heavy-quark degrees of freedom have been integrated out. This corresponds to take the $m_Q \to \infty$ limit.

We have regularized the infrared divergences according to the conventional dimensional regularization method, i.e. we have set the space-time dimensions $D = 4 - 2\epsilon$.

The finite soft-virtual term, obtained from the sum of the divergent virtual contributions and of the integral over the radiation variables of the counter-terms is given by (see eq. (2.99) of ref. [9])

$$\mathcal{V}_{gg} = \frac{\alpha_{\rm S}}{2\pi}\left[-\left(\frac{11}{3}C_{\rm A} - \frac{4}{3}T_{\rm F}n_f\right)\log\frac{\mu_{\rm F}^2}{\mu_{\rm R}^2} + \frac{11}{3}C_{\rm A} + \frac{2\pi^2}{3}C_{\rm A}\right]\mathcal{B}_{gg}\,. \tag{2.22}$$

In deriving this equation we have set $\xi_c = 1$. We indicate with $\mu_{\rm R}$ and $\mu_{\rm F}$ the renormalization and factorization scales, respectively.

JHEP04(2009)002

2.2.3 Real corrections

At NLO, there are four subprocesses that contribute to Higgs boson production: $gg \to Hg$, $gq \to Hq$, $qg \to Hq$ and $q\bar{q} \to Hg$, where q runs over all possible quark and antiquark flavours and q and $\bar{q}$ are conjugate in flavour. The respective squared amplitudes, averaged over the incoming helicities and colours and multiplied by the flux factor $1/(2s)$ are given by

$$\mathcal{R}_{gg} = \frac{\alpha_S^3}{12\pi} \frac{G_F}{\sqrt{2}} \frac{1}{2s} \frac{s^4 + t^4 + u^4 + M^8}{stu}, \tag{2.23}$$

$$\mathcal{R}_{gq} = -\frac{\alpha_S^3}{27\pi} \frac{G_F}{\sqrt{2}} \frac{1}{2s} \frac{s^2 + u^2}{t}, \tag{2.24}$$

$$\mathcal{R}_{qg} = -\frac{\alpha_S^3}{27\pi} \frac{G_F}{\sqrt{2}} \frac{1}{2s} \frac{s^2 + t^2}{u}, \tag{2.25}$$

$$\mathcal{R}_{q\bar{q}} = \frac{8\,\alpha_S^3}{81\pi} \frac{G_F}{\sqrt{2}} \frac{1}{2s} \frac{t^2 + u^2}{s}, \tag{2.26}$$

where

$$s = \left(k_\oplus + k_\ominus\right)^2 = \frac{M^2}{1-\xi}, \quad t = \left(k_\ominus - k_2\right)^2 = -\frac{s}{2}\,\xi\,(1+y), \quad u = \left(k_\oplus - k_2\right)^2 = -\frac{s}{2}\,\xi\,(1-y). \tag{2.27}$$

In terms of the FKS variables we then have

$$\mathcal{R}_{gg} = \frac{\alpha_S^3}{12\pi} \frac{G_F}{\sqrt{2}} \frac{1}{4} \left[8 + \left(y^4 + 6y^2 + 1\right)\xi^4 + 8(1-\xi)^4\right] \frac{1}{\xi^2(1-y^2)}, \tag{2.28}$$

$$\mathcal{R}_{gq} = \frac{\alpha_S^3}{27\pi} \frac{G_F}{\sqrt{2}} \frac{1}{4} \left[4 + (1-y)^2\xi^2\right] \frac{1}{\xi(1+y)}, \tag{2.29}$$

$$\mathcal{R}_{qg} = \frac{\alpha_S^3}{27\pi} \frac{G_F}{\sqrt{2}} \frac{1}{4} \left[4 + (1+y)^2\xi^2\right] \frac{1}{\xi(1-y)}, \tag{2.30}$$

$$\mathcal{R}_{q\bar{q}} = \frac{8\,\alpha_S^3}{81\pi} \frac{G_F}{\sqrt{2}} \frac{1}{4} \left[\xi^2\left(1+y^2\right)\right], \tag{2.31}$$

where the singular behavior for a soft ($\xi \to 0$) or collinear gluon ($y \to \pm 1$) is clearly manifest. Notice that the contribution $\mathcal{R}_{q\bar{q}}$ is not singular and has no underlying Born.

2.2.4 Collinear remnants

After the subtraction of the initial-state collinear singularities into the parton distribution functions, finite collinear remnants are left over. The kinematics of these terms is Born-like. More precisely, we can introduce two sets of variables, $\bar{\mathbf{\Phi}}_{1,\circledast} = \left\{M^2, Y, z\right\}$, such that momentum conservation reads

$$z\,x_\oplus K_\oplus + x_\ominus K_\ominus = k_1 \tag{2.32}$$

for the $\oplus$ direction and

$$x_\oplus K_\oplus + z\,x_\ominus K_\ominus = k_1 \tag{2.33}$$

for the $\ominus$ one. We can then associate an underlying Born configuration $\bar{\mathbf{\Phi}}_1$ such that

$$\bar{k}_\oplus = z\,x_\oplus K_\oplus, \qquad \bar{k}_\ominus = x_\ominus K_\ominus, \qquad \bar{k}_1 = k_1 \tag{2.34}$$

JHEP04(2009)002

for the $\oplus$ direction, and

$$\bar{k}_\oplus = x_\oplus K_\oplus\,, \qquad \bar{k}_\ominus = z\, x_\ominus K_\ominus\,, \qquad \bar{k}_1 = k_1 \tag{2.35}$$

for the $\ominus$ one.

The collinear remnants are given in eq. (2.102) of ref. [9], where we have fixed $\xi_c = 1$ and $\delta_I = 2$ and chosen the $\overline{\text{MS}}$ renormalization scheme. For the $\oplus$ direction and for the two different real-term contributions, they are given by

$$\begin{aligned}\mathcal{G}^{gg}_{\oplus}\left(\bar{\mathbf{\Phi}}_{1,\oplus}\right) = \frac{\alpha_{\text{S}}}{2\pi}\, C_{\text{F}} \Bigg\{ (1-z)\frac{1+(1-z)^2}{z}\left[\left(\frac{1}{1-z}\right)_+ \log\left(\frac{M^2}{z\mu_F^2}\right)\right.\\ \left. + 2\left(\frac{\log(1-z)}{1-z}\right)_+\right] + z\Bigg\}\,\mathcal{B}_{gg}\,,\end{aligned} \tag{2.36}$$

$$\begin{aligned}\mathcal{G}^{gg}_{\oplus}\left(\bar{\mathbf{\Phi}}_{1,\oplus}\right) = \frac{\alpha_{\text{S}}}{2\pi}\, 2C_{\text{A}}\left[z + \frac{(1-z)^2}{z} + z(1-z)^2\right]\\ \times\left[\left(\frac{1}{1-z}\right)_+ \log\left(\frac{M^2}{z\mu_F^2}\right) + 2\left(\frac{\log(1-z)}{1-z}\right)_+\right]\mathcal{B}_{gg}\,.\end{aligned} \tag{2.37}$$

The other two collinear remnants, $\mathcal{G}^{qg}_{\ominus}(\bar{\mathbf{\Phi}}_{1,\ominus})$ and $\mathcal{G}^{gg}_{\ominus}(\bar{\mathbf{\Phi}}_{1,\ominus})$, have the same functional form of $\mathcal{G}^{qg}_{\oplus}\left(\bar{\mathbf{\Phi}}_{1,\oplus}\right)$ and $\mathcal{G}^{gg}_{\oplus}\left(\bar{\mathbf{\Phi}}_{1,\oplus}\right)$ respectively, since $\mathcal{B}_{gg}$ only depends upon k_1^2.

3 POWHEG implementation

3.1 Generation of the Born variables

The first step in the POWHEG implementation is the generation of the Born kinematics. According to ref. [9], we introduce the $\bar{B}\left(\bar{\mathbf{\Phi}}_1\right)$ function, defined as

$$\begin{aligned}\bar{B}\left(\bar{\mathbf{\Phi}}_1\right) = B_{gg}\left(\bar{\mathbf{\Phi}}_1\right) + V_{gg}\left(\bar{\mathbf{\Phi}}_1\right)\\ + \int d\Phi_{\text{rad}}\left\{\hat{R}_{gg}\left(\bar{\mathbf{\Phi}}_1,\Phi_{\text{rad}}\right) + \sum_q\left[\hat{R}_{qg}\left(\bar{\mathbf{\Phi}}_1,\Phi_{\text{rad}}\right) + \hat{R}_{gq}\left(\bar{\mathbf{\Phi}}_1,\Phi_{\text{rad}}\right)\right]\right\}\\ + \int_{\bar{x}_\oplus}^1 \frac{dz}{z}\left[G^{gg}_{\oplus}(\bar{\mathbf{\Phi}}_{1,\oplus}) + \sum_q G^{qg}_{\oplus}(\bar{\mathbf{\Phi}}_{1,\oplus})\right] + \int_{\bar{x}_\ominus}^1 \frac{dz}{z}\left[G^{gg}_{\ominus}(\bar{\mathbf{\Phi}}_{1,\ominus}) + \sum_q G^{qg}_{\ominus}(\bar{\mathbf{\Phi}}_{1,\ominus})\right],\end{aligned} \tag{3.1}$$

where

$$B_{gg}\left(\bar{\mathbf{\Phi}}_1\right) = \mathcal{B}_{gg}\left(\bar{\mathbf{\Phi}}_1\right)\,\mathcal{L}_{gg}(\bar{x}_\oplus,\bar{x}_\ominus)\,, \tag{3.2}$$

$$V_{gg}\left(\bar{\mathbf{\Phi}}_1\right) = \mathcal{V}_{gg}\left(\bar{\mathbf{\Phi}}_1\right)\,\mathcal{L}_{gg}(\bar{x}_\oplus,\bar{x}_\ominus)\,, \tag{3.3}$$

$$\hat{R}_{gg}(\bar{\mathbf{\Phi}}_1,\Phi_{\text{rad}}) = \hat{\mathcal{R}}_{gg}(\bar{\mathbf{\Phi}}_1,\Phi_{\text{rad}})\,\mathcal{L}_{gg}(x_\oplus,x_\ominus)\,, \tag{3.4}$$

$$\hat{R}_{gq}(\bar{\mathbf{\Phi}}_1,\Phi_{\text{rad}}) = \hat{\mathcal{R}}_{gq}(\bar{\mathbf{\Phi}}_1,\Phi_{\text{rad}})\,\mathcal{L}_{gq}(x_\oplus,x_\ominus)\,, \tag{3.5}$$

$$\hat{R}_{qg}(\bar{\mathbf{\Phi}}_1,\Phi_{\text{rad}}) = \hat{\mathcal{R}}_{qg}(\bar{\mathbf{\Phi}}_1,\Phi_{\text{rad}})\,\mathcal{L}_{qg}(x_\oplus,x_\ominus)\,, \tag{3.6}$$

$$G^{gg}_{\oplus}(\bar{\mathbf{\Phi}}_{1,\oplus}) = \mathcal{G}^{gg}_{\oplus}(\bar{\mathbf{\Phi}}_{1,\oplus})\,\mathcal{L}_{gg}\left(\frac{\bar{x}_\oplus}{z},\bar{x}_\ominus\right), \tag{3.7}$$

JHEP04(2009)002

$$G^{qg}_{\oplus}(\bar{\mathbf{\Phi}}_{1,\oplus}) = \mathcal{G}^{qg}_{\oplus}(\bar{\mathbf{\Phi}}_{1,\oplus})\,\mathcal{L}_{qg}\Big(\frac{\bar{x}_{\oplus}}{z},\bar{x}_{\ominus}\Big)\,, \tag{3.8}$$

$$G^{gg}_{\ominus}(\bar{\mathbf{\Phi}}_{1,\ominus}) = \mathcal{G}^{gg}_{\ominus}(\bar{\mathbf{\Phi}}_{1,\ominus})\,\mathcal{L}_{gg}\Big(\bar{x}_{\oplus},\frac{\bar{x}_{\ominus}}{z}\Big)\,, \tag{3.9}$$

$$G^{gq}_{\ominus}(\bar{\mathbf{\Phi}}_{1,\ominus}) = \mathcal{G}^{gq}_{\ominus}(\bar{\mathbf{\Phi}}_{1,\ominus})\,\mathcal{L}_{gq}\Big(\bar{x}_{\oplus},\frac{\bar{x}_{\ominus}}{z}\Big)\,, \tag{3.10}$$

with $x_{\oplus}, x_{\ominus}$ given in eq. (2.12) and the luminosity $\mathcal{L}$ is defined in terms of the parton distribution functions $f^{\circledast}_{f}(x_{\circledast},\mu^2_{\rm F})$

$$\mathcal{L}_{ff'}\ (x_{\oplus},x_{\ominus}\ ) = f^{\oplus}_{f}\left(x_{\oplus},\mu^2_{\rm F}\right)\ f^{\ominus}_{f'}\left(x_{\ominus},\mu^2_{\rm F}\right)\ . \tag{3.11}$$

Observe that the $\mathcal{R}_{q\bar{q}}$ term does not appear in $\bar{B}$, since it does not have a valid underlying Born. It is just generated separately, as described at the end of this section.

All the integrals appearing in eq. (3.1) are finite. In fact, according the the FKS subtraction scheme, the hatted functions

$$\hat{\mathcal{R}}_{ij} = \frac{1}{\xi}\left\{\frac{1}{2}\left(\frac{1}{\xi}\right)_+\left[\left(\frac{1}{1-y}\right)_+ + \left(\frac{1}{1+y}\right)_+\right]\right\}\left[(1-y^2)\ \xi^2\,\mathcal{R}_{ij}\right] \tag{3.12}$$

have only integrable divergences. Some care should still be used when dealing with the plus distributions. In order to illustrate this, we explicitly show how to deal with the $\mathcal{R}_{gg}$ term, that is the most singular one. According to eq. (3.12), it can be written

$$\hat{\mathcal{R}}_{gg} = \frac{\alpha_{\rm S}^3}{12\pi}\,\frac{G_F}{\sqrt{2}}\left[2+\frac{y^4+6y^2+1}{4}\xi^4+2(1-\xi)^4\right]\left\{\frac{1}{2}\left(\frac{1}{\xi}\right)_+\left[\left(\frac{1}{1-y}\right)_+ + \left(\frac{1}{1+y}\right)_+\right]\right\}\frac{1}{\xi}. \tag{3.13}$$

Inserting now the expression (2.19) of $d\Phi_{\rm rad}$ into eq. (3.1), we have

$$\int d\Phi_{\rm rad}\,\mathcal{L}_{gg}(x_{\oplus},x_{\ominus})\,\hat{\mathcal{R}}_{gg} = \frac{M^2}{(4\pi)^3}\int_{-1}^{1}dy\int_0^{\xi_{\rm M}(y)}d\xi\,\frac{\xi}{(1-\xi)^2}\int_0^{2\pi}d\phi\,\mathcal{L}_{gg}(x_{\oplus},x_{\ominus})\,\hat{\mathcal{R}}_{gg}\,, \tag{3.14}$$

where $\xi_{\rm M}(y)$ is given in eq. (2.14). The integration over the azimuthal angle ϕ is straightforward, giving an overall multiplicative factor of 2π. Considering then the $(1/(1-y))_+$ term only, we get an integral of the form

$$I = \int_{-1}^{1}dy\int_0^{\xi_{\rm M}(y)}d\xi\left(\frac{1}{\xi}\right)_+\left(\frac{1}{1-y}\right)_+ f(\xi,y)\,\mathcal{L}_{gg}(x_{\oplus},x_{\ominus}) \tag{3.15}$$

where

$$f(\xi,y) = \frac{\alpha_{\rm S}^3}{12\pi}\,\frac{G_F}{\sqrt{2}}\left[2+\frac{y^4+6y^2+1}{4}\xi^4+2(1-\xi)^4\right]\frac{1}{2}\,\frac{M^2}{(4\pi)^3}\,\frac{2\pi}{(1-\xi)^2}\,. \tag{3.16}$$

Recalling the definition of the plus distributions

$$\int_0^1 d\xi\left(\frac{1}{\xi}\right)_+ f(\xi) = \int_0^1 d\xi\,\frac{f(\xi)-f(0)}{\xi}\,, \tag{3.17}$$

$$\int_{-1}^1 dy\left(\frac{1}{1-y}\right)_+ f(y) = \int_{-1}^1 dy\,\frac{f(y)-f(1)}{1-y}\,, \tag{3.18}$$

JHEP04(2009)002

and making the change of variable

$$\xi = \xi_{\rm M}(y)\,\tilde{\xi}\,, \tag{3.19}$$

we are left with

$$\begin{aligned}
I = & \int_{-1}^{1} dy \left(\frac{1}{1-y}\right)_+ \int_0^1 d\tilde{\xi} \left(\frac{1}{\tilde{\xi}}\right)_+ f\left(\xi, y\right)\, \mathcal{L}_{gg}\left(x_\oplus, x_\ominus\right) \\
& + \int_{-1}^{1} dy \left(\frac{1}{1-y}\right)_+ f(0,y)\, \log \xi_{\rm M}(y)\, \mathcal{L}_{gg}(\bar{x}_\oplus, \bar{x}_\ominus) \\
= & \int_{-1}^{1} dy \left(\frac{1}{1-y}\right)_+ \int_0^1 d\tilde{\xi}\, \frac{1}{\tilde{\xi}} \Big[f\left(\xi, y\right) \mathcal{L}_{gg}(x_\oplus, x_\ominus) - f\left(0, y\right) \mathcal{L}_{gg}(\bar{x}_\oplus, \bar{x}_\ominus) \Big] \\
& + \int_{-1}^{1} dy\, \frac{1}{1-y} \Big[f(0,y)\, \log \xi_{\rm M}(y) - f(0,1)\, \log \xi_{\rm M}(1) \Big] \mathcal{L}_{gg}(\bar{x}_\oplus, \bar{x}_\ominus) \\
= & \int_0^1 d\tilde{y} \int_0^1 d\tilde{\xi}\, \frac{1}{1-\tilde{y}}\, \frac{1}{\tilde{\xi}} \Bigg\{ \Big[f\left(\xi, y\right) \mathcal{L}_{gg}(x_\oplus, x_\ominus) - f\left(0, y\right) \mathcal{L}_{gg}(\bar{x}_\oplus, \bar{x}_\ominus) \Big] \\
& - \left[f\left(\xi, 1\right) \mathcal{L}_{gg}\left(\frac{\bar{x}_\oplus}{1-\xi}, \bar{x}_\ominus\right) - f\left(0, 1\right) \mathcal{L}_{gg}(\bar{x}_\oplus, \bar{x}_\ominus) \right] \Bigg\} \\
& + \int_0^1 d\tilde{y}\, \frac{1}{1-\tilde{y}} \Big[f(0,y)\, \log \xi_{\rm M}(y) - f(0,1)\, \log \xi_{\rm M}(1) \Big] \mathcal{L}_{gg}(\bar{x}_\oplus, \bar{x}_\ominus)\,,
\end{aligned} \tag{3.20}$$

where we have used the expression of $x_{\textcircled{\scriptsize +}}$ of eq. (2.12) and $\xi_{\rm M}(1) = 1 - \bar{x}_\oplus$ (see eq. (2.14)). In the last line we have made the further change of variable

$$y = -1 + 2\,\tilde{y}\,, \tag{3.21}$$

so that all radiation variables are mapped into a cubic unit volume. The integral I is now manifestly finite and can be computed numerically.

The same manipulations should be applied to the z integration of the collinear remnants in eq. (3.1). For example, concentrating on the two plus distributions in the $\mathcal{G}_\oplus^{gg}$ term, we have to deal with integrals of the form

$$\int_{\bar{x}_\oplus}^1 dz \left(\frac{1}{1-z}\right)_+ f(z) = \log(1-\bar{x}_\oplus) f(1) + \int_0^1 d\tilde{\xi}\, \frac{f(z) - f(1)}{1-\tilde{\xi}}\,, \tag{3.22}$$

$$\int_{\bar{x}_\oplus}^1 dz \left(\frac{\log(1-z)}{1-z}\right)_+ f(z) = \frac{1}{2} \log^2(1-\bar{x}_\oplus) f(1) + \int_0^1 d\tilde{\xi}\, \frac{\log(1-z)}{1-\tilde{\xi}} \left[f(z) - f(1)\right], \tag{3.23}$$

where $f(z)$ is finite in the $z \to 1$ limit and we have made the change of variable

$$z = \bar{x}_\oplus + \tilde{\xi}\,(1 - \bar{x}_\oplus)\,. \tag{3.24}$$

At the end of this procedure, the most general form one can obtain for $\bar{B}$ is

$$\bar{B}\big(\bar{\mathbf{\Phi}}_1\big) = D\big(\bar{\mathbf{\Phi}}_1\big) + \int_0^1 d\tilde{\xi}\, E\Big(\bar{\mathbf{\Phi}}_1, \tilde{\xi}\Big) + \int_0^1 d\tilde{y} \int_0^1 d\tilde{\xi}\, F\Big(\bar{\mathbf{\Phi}}_1, \tilde{\xi}, \tilde{y}\Big)\,, \tag{3.25}$$

JHEP04(2009)002

and we can define the function

$$\tilde{B}\Big(\bar{\mathbf{\Phi}}_1,\tilde{\xi},\tilde{y}\Big) = D\big(\bar{\mathbf{\Phi}}_1\big) + E\Big(\bar{\mathbf{\Phi}}_1,\tilde{\xi}\Big) + F\Big(\bar{\mathbf{\Phi}}_1,\tilde{\xi},\tilde{y}\Big)\,, \tag{3.26}$$

so that

$$\bar{B}\big(\bar{\mathbf{\Phi}}_1\big) = \int_0^1 d\tilde{y} \int_0^1 d\tilde{\xi}\, \tilde{B}\Big(\bar{\mathbf{\Phi}}_1,\tilde{\xi},\tilde{y}\Big)\,. \tag{3.27}$$

In order to generate the underlying Born kinematics, we first compute the two distinct contributions to the total cross section, defined by

$$\sigma_{\rm tot} = \sigma_{\bar{B}} + \sum_q \sigma_{R_{q\bar{q}}}\,, \tag{3.28}$$

where

$$\begin{aligned}\sigma_{\bar{B}} &= \int d\bar{\mathbf{\Phi}}_1\, \bar{B}\big(\bar{\mathbf{\Phi}}_1\big)\,,\\ \sigma_{R_{q\bar{q}}} &= \int d\bar{\mathbf{\Phi}}_1\, d\Phi_{\rm rad}\, R_{q\bar{q}}(\bar{\mathbf{\Phi}}_1,\Phi_{\rm rad})\,,\end{aligned} \tag{3.29}$$

and

$$R_{q\bar{q}}(\bar{\mathbf{\Phi}}_1,\Phi_{\rm rad}) = \mathcal{R}_{q\bar{q}}(\bar{\mathbf{\Phi}}_1,\Phi_{\rm rad})\,\mathcal{L}_{q\bar{q}}(x_\oplus,x_\ominus)\,. \tag{3.30}$$

We then decide whether the event is a $\bar{B}$ event or a $R_{q\bar{q}}$ one, with a probability equal to $\sigma_{\bar{B}}/\sigma_{\rm tot}$ and $\sigma_{R_{q\bar{q}}}/\sigma_{\rm tot}$ respectively. In case of a $\bar{B}$ event, the generation of the Born variables $\bar{\mathbf{\Phi}}_1$ is performed by using the integrator-unweighter program `MINT` [22] that, after a single integration of the function $\tilde{B}(\bar{\mathbf{\Phi}}_1,\tilde{\xi},\tilde{y})$ over the Born and radiation variables, can generate a set of values for the variables $\{\bar{\mathbf{\Phi}}_1,\tilde{\xi},\tilde{y}\}$, distributed according to the weight $\tilde{B}(\bar{\mathbf{\Phi}}_1,\tilde{\xi},\tilde{y})$. We then keep the $\bar{\mathbf{\Phi}}_1$ generated values only, and neglect all the others, which corresponds to integrate over them. The event is then further processed, to generate the radiation variables, as illustrated in the following section. In case of a $R_{q\bar{q}}$ event, one uses the same method used for the $\bar{B}$ case, except that, at the end, one keeps the whole set of Born plus radiation variables, that fully defines the kinematics of a real event. In this last case, one does not need to do anything else, and the event is passed to the Les Houches Interface, to be further showered by the Monte Carlo program.

3.2 Generation of the radiation variables

Radiation kinematics is generated using the `POWHEG` Sudakov form factor

$$\Delta\big(\bar{\mathbf{\Phi}}_1,p_{\rm T}\big) = \exp\left\{-\int d\Phi_{\rm rad}\,\frac{R\left(\bar{\mathbf{\Phi}}_1,\Phi_{\rm rad}\right)}{B\left(\bar{\mathbf{\Phi}}_1\right)}\,\theta(k_{\rm T}-p_{\rm T})\right\}, \tag{3.31}$$

where we have defined

$$R\left(\bar{\mathbf{\Phi}}_1,\Phi_{\rm rad}\right) = R_{gg}\left(\bar{\mathbf{\Phi}}_1,\Phi_{\rm rad}\right) + \sum_q \left[R_{qg}\left(\bar{\mathbf{\Phi}}_1,\Phi_{\rm rad}\right) + R_{gq}\left(\bar{\mathbf{\Phi}}_1,\Phi_{\rm rad}\right)\right]\,, \tag{3.32}$$

$$B\big(\bar{\mathbf{\Phi}}_1\big) = B_{gg}\big(\bar{\mathbf{\Phi}}_1\big)\,, \tag{3.33}$$

and

$$k_{\mathrm{T}}^2 = \frac{s}{4}\,\xi^2\,(1-y^2) = \frac{M^2}{4(1-\xi)}\,\xi^2\,(1-y^2) \tag{3.34}$$

is the exact squared transverse momentum of the radiated parton. The factorization and renormalization scales in eq. (3.31) should be taken equal to k_{T}^2, in order to recover the correct leading logarithm (LL) Sudakov behavior.[2]

To generate the radiation variables, we use the veto method. This requires to find a simple upper bound for the integrand in eq. (3.31)

$$\frac{M^2}{(4\pi)^3}\,\frac{\xi}{(1-\xi)^2}\,\frac{R\big(\bar{\mathbf{\Phi}}_1,\Phi_{\mathrm{rad}}\big)}{B\big(\bar{\mathbf{\Phi}}_1\big)}\,. \tag{3.35}$$

A suitable upper bounding function is given by

$$U = N\,\frac{\alpha_{\mathrm{S}}\big(k_{\mathrm{T}}^2\big)}{\xi\,(1-y^2)}\,, \tag{3.36}$$

where N is determined by spanning randomly the whole phase space and imposing that U is larger than the integrand function. The generation of the event according to the bound (3.36) is documented in great detail in appendix D of ref. [23], and we do not repeat it here.

The POWHEG differential cross section for the generation of the hardest event is given by

$$\begin{aligned} d\sigma \;=\; & \bar{B}(\bar{\mathbf{\Phi}}_1)\,d\bar{\mathbf{\Phi}}_1\left\{\Delta\big(\bar{\mathbf{\Phi}}_1,p_{\mathrm{T}}^{\mathrm{min}}\big)+\Delta\big(\bar{\mathbf{\Phi}}_1,p_{\mathrm{T}}\big)\;\frac{R\left(\bar{\mathbf{\Phi}}_1,\Phi_{\mathrm{rad}}\right)}{B\big(\bar{\mathbf{\Phi}}_1\big)}\,d\Phi_{\mathrm{rad}}\right\} \\ & +\;\sum_q R_{q\bar{q}}\left(\bar{\mathbf{\Phi}}_1,\Phi_{\mathrm{rad}}\right)d\bar{\mathbf{\Phi}}_1 d\Phi_{\mathrm{rad}}\,, \end{aligned} \tag{3.37}$$

where the last term in the sum is the non-singular real contribution. In the $\bar{B}$ and $R_{q\bar{q}}$ functions, the renormalization and factorization scales, μ_{R} and μ_{F}, should be taken of the order of the hard scale of the process, i.e. the Higgs boson mass or its transverse mass. During the generation of radiation, the two scales should instead be taken equal to the transverse momentum of the produced radiation, in order to recover the correct Sudakov form factor.

We remark that, in the formula for the strong coupling constant used for the generation of radiation, we have properly taken into account the heavy-flavour thresholds. That is to say, when the renormalization scale μ_{R} crosses a heavy-flavour mass threshold, we change the number of active flavours accordingly. Furthermore, as discussed in refs. [9, 10], we use a rescaled value $\Lambda_{\mathrm{MC}} = 1.569\,\Lambda_{\overline{\mathrm{MS}}}^{(5)}$ in the expression for α_{S}, in order to achieve next-to-leading logarithmic accuracy in the Sudakov form factor (see section 4.4 for more details).

[2] We will show in section 4.4 how it is possible to reach next-to-leading logarithmic accuracy for this particular process.

JHEP04(2009)002

4 Results

In this section we present our results, obtained for the Tevatron and the LHC, and the comparison done with MC@NLO and PYTHIA. We have used the CTEQ6M [24] set for the parton distribution functions and the corresponding returned value $\Lambda^{(5)}_{\overline{\rm MS}} = 0.226\,\text{GeV}$. In the generation of the radiation, we have fixed the lower cutoff of the transverse momentum to the value $p_{\rm T}^{\rm min} = \sqrt{5}\,\Lambda_{\rm MC}$. The renormalization and factorization scales have been taken equal to the Higgs boson transverse mass $m_{\rm T}^H = \sqrt{m_H^2 + (p_{\rm T}^H)^2}$.

No acceptance cuts have been applied in any of the following plots.

4.1 POWHEG - MC@NLO comparison

We have compared our results with MC@NLO, the only existing program where NLO Higgs boson production via gluon fusion is merged with a shower Monte Carlo program. Since MC@NLO uses only the HERWIG [5, 6] angular-ordered shower, we have also interfaced POWHEG with HERWIG, in order to minimize effects due to differences in the shower and hadronization algorithms.

MC@NLO generates the Higgs boson virtuality M^2 according to the Breit-Wigner form

$$\frac{1}{\pi}\frac{m_H\,\Gamma_H}{\left(M^2 - m_H^2\right)^2 + (m_H\,\Gamma_H)^2}\,. \tag{4.1}$$

For the purpose of this comparison we have thus used the same form. We have considered two different sets of values for the Higgs boson mass and width: $m_H = 120\,\text{GeV}$ with $\Gamma_H = 3.605\,\text{MeV}$ and $m_H = 400\,\text{GeV}$ with $\Gamma_H = 28.89\,\text{GeV}$.

Both in POWHEG and in MC@NLO there is the option to retain the full top-mass dependence in the Born cross section, i.e. to use a finite τ_Q value in eq. (2.20). We have then the choice to generate our Born variables by fixing $m_t = 171\,\text{GeV}$ in the $\bar{B}$ term in eq. (3.1) or by sending $m_t \to \infty$. Since we have computed the real-radiation term only in the $m_t \to \infty$ limit, we have to use the same limit in the calculation of the Born term in the Sudakov form factor (3.31), in order to recover the correct Altarelli-Parisi behavior when the collinear limit is approached.

4.1.1 Tevatron results

In figure 1 we show a comparison between POWHEG and MC@NLO for the rapidity, invariant mass and transverse-momentum distributions of a Higgs boson with mass $m_H = 120\,\text{GeV}$, at the Tevatron $p\bar{p}$ collider. The lowest order m_t-dependence is retained. A blowup of the transverse-momentum distribution near the low-$p_{\rm T}$ region is also shown. There is good agreement between the two programs, except for the transverse momentum distribution at high $p_{\rm T}$ (we will comment more on this issue in section 4.3). In figure 2 we compare the leading jet rapidity and the difference in the rapidity of the leading jet and the Higgs boson. The jet is defined using the SISCONE algorithm [25] as implemented in the FASTJET package [26], setting the jet radius $R = 0.7$ and the overlapping fraction $f = 0.5$. As in previous POWHEG implementations, we notice a dip in the MC@NLO jet rapidity distribution, which is enhanced in the difference. We have already extensively discussed this fact in

JHEP04(2009)002

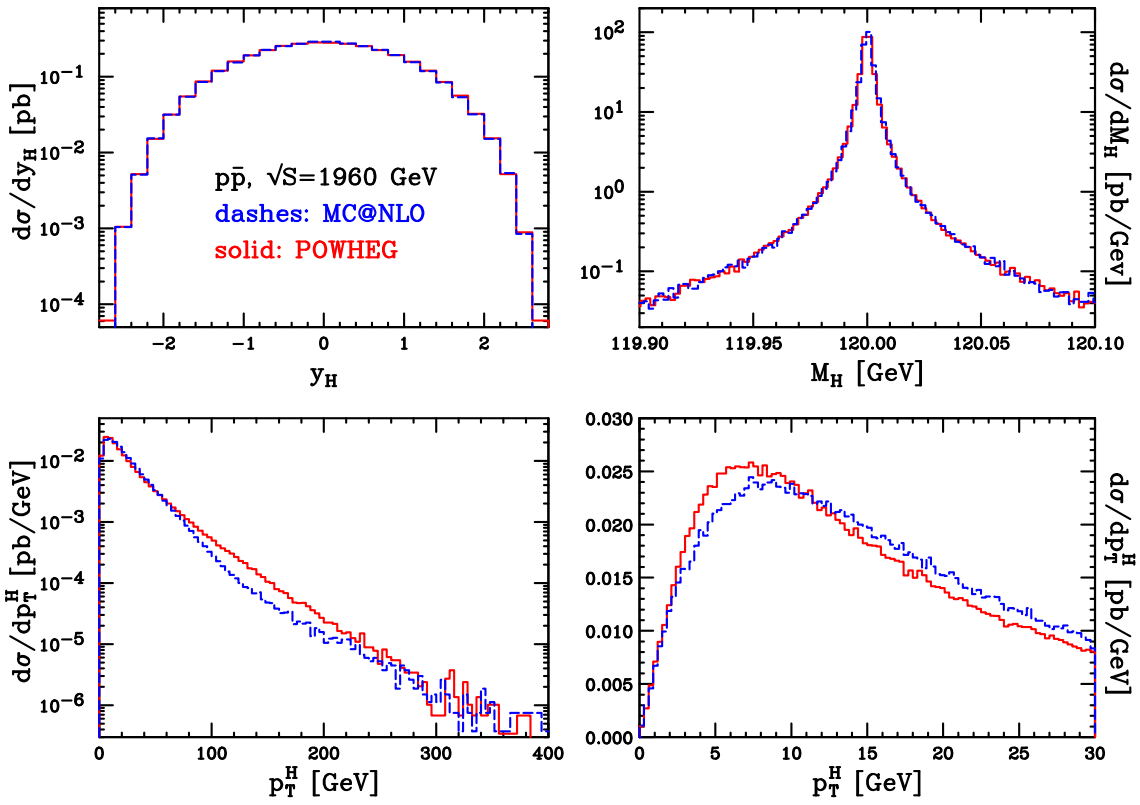

Figure 1. Comparison between POWHEG and MC@NLO for the rapidity, invariant mass and transverse-momentum distributions of a Higgs boson with $m_H = 120\,\text{GeV}$, at Tevatron $p\bar{p}$ collider.

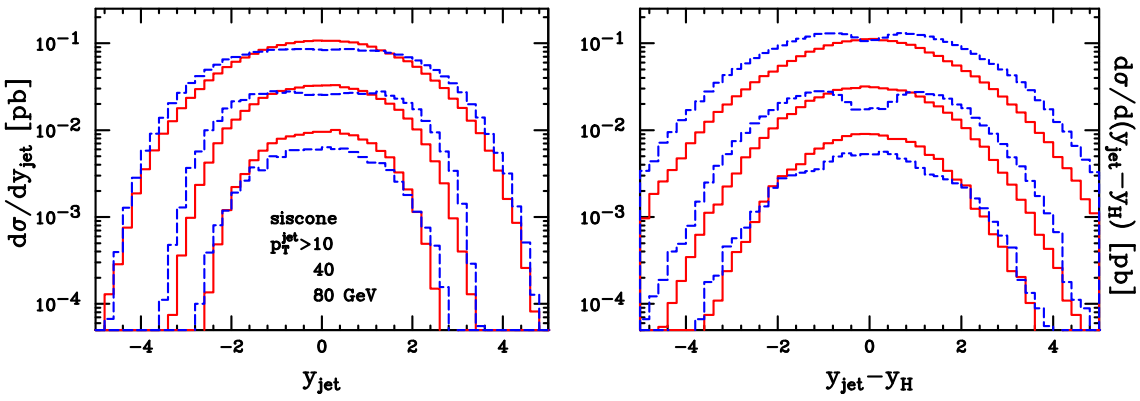

Figure 2. Comparison between POWHEG and MC@NLO for the rapidity of the leading jet and the rapidity difference of the Higgs boson and the leading jet, defined according to the SISCONE algorithm, with different jet cuts.

JHEP04(2009)002

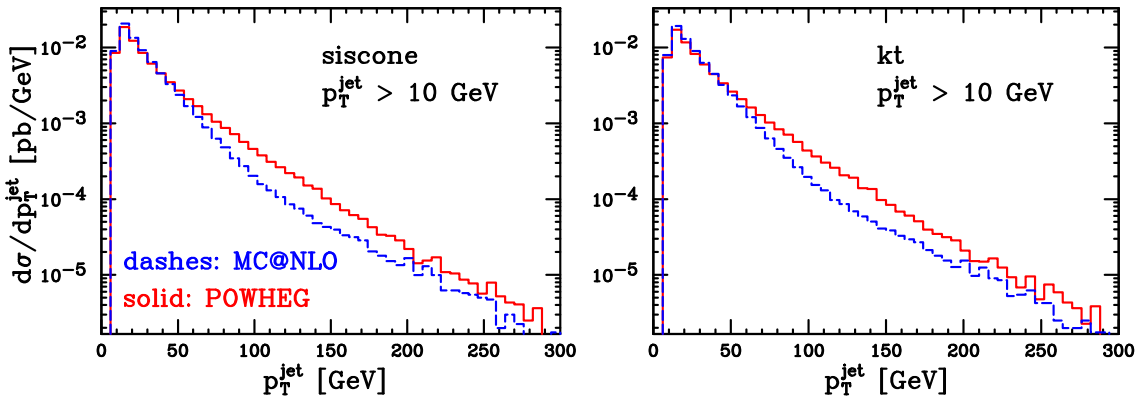

Figure 3. Comparison between POWHEG and MC@NLO for the transverse-momentum distributions of the leading jet, defined according to the SISCONE and the KT jet algorithms.

section 4.3 of ref. [14]. In figure 3, we compare the transverse-momentum distributions of the leading jet, reconstructed with the SISCONE and the k_T algorithms (included in FASTJET). A lower 10 GeV cut on jet transverse momentum is imposed. The high-p_T discrepancy reflects the same behavior found for the Higgs boson transverse-momentum distribution (see section 4.3).

4.1.2 LHC results

From figure 4 to 6 we carry out a similar analysis for the LHC pp collider. The difference in the hardness of the p_T distributions is more evident here than at the Tevatron. The other plots show instead a good agreement between the two codes, apart from the aforementioned dip in the leading-jet rapidity distributions. We have also made some comparisons with a different value of the Higgs boson mass. We have chosen $m_H = 400\,\text{GeV}$, where the ratio between the Born cross sections evaluated with $m_t = 171\,\text{GeV}$ and $m_t \to \infty$ is close to its maximum value and roughly equals 3. The results are shown in figure 7 and 8. We see that, in this case, the dip in the rapidity of the hardest jet in MC@NLO is extremely marked. In the study of ref. [17], carried out in the framework of heavy-flavour production, the origin of the rapidity dip was tracked back to an even stronger dip in the pure HERWIG distribution, that the MC@NLO correction was not able to properly fill. The same pattern is also observed in the present context, as can be seen in figure 9.

4.2 POWHEG - PYTHIA comparison

We now compare POWHEG and PYTHIA. The Higgs boson production implementation in PYTHIA includes matrix-element corrections, so that the p_T distribution of the Higgs boson is accurate at large p_T. In our comparisons, we always normalize the PYTHIA results to the full NLO cross section of POWHEG. We use the new p_T-ordered shower defined in the PYEVNW routine of PYTHIA, that should be more appropriate when interfacing to POWHEG.

The only difference with respect to the POWHEG-MC@NLO comparisons is in the generation

JHEP04(2009)002

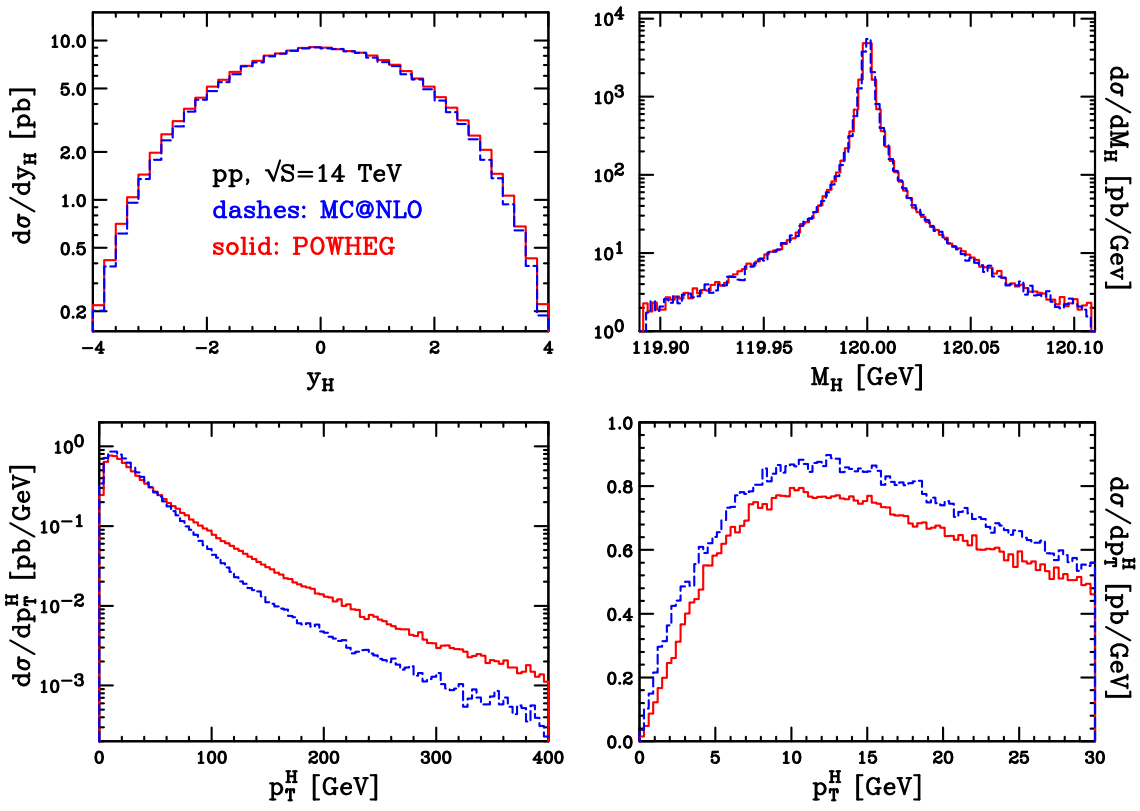

Figure 4. Comparison between POWHEG and MC@NLO for the rapidity, invariant mass and transverse-momentum distributions of a Higgs boson with $m_H = 120\,\text{GeV}$, at the LHC pp collider.

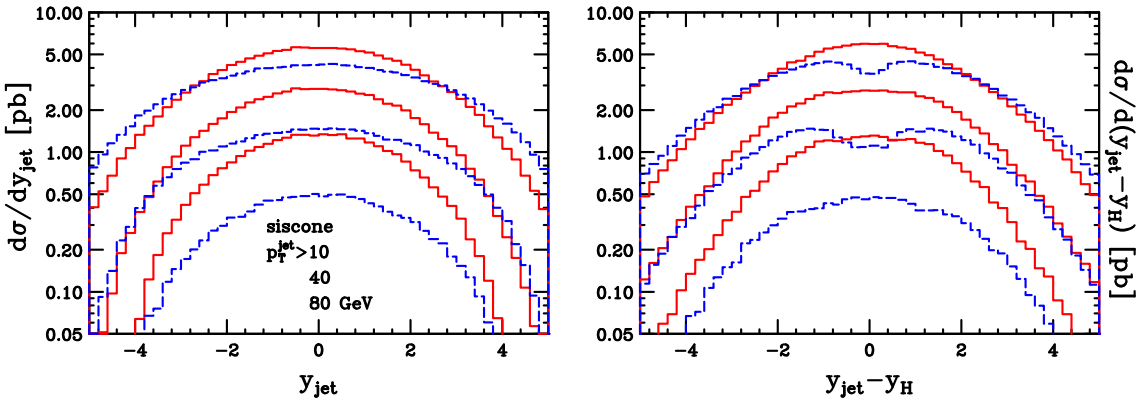

Figure 5. Comparison between POWHEG and MC@NLO for the rapidity of the leading jet and the rapidity difference of the Higgs boson and the leading jet, defined according to the SISCONE algorithm, with different jet cuts.

JHEP04(2009)002

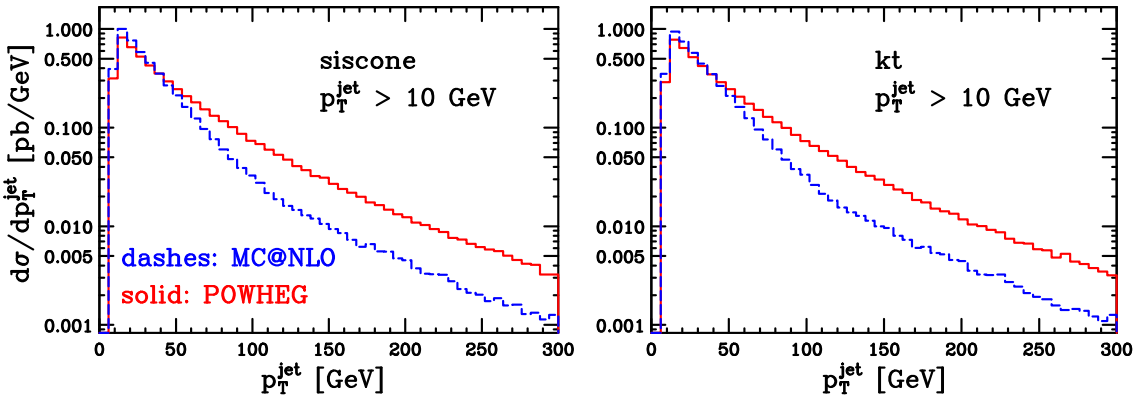

Figure 6. Comparison between POWHEG and MC@NLO for the transverse-momentum distributions of the leading jet, defined according to the SISCONE and the KT algorithms.

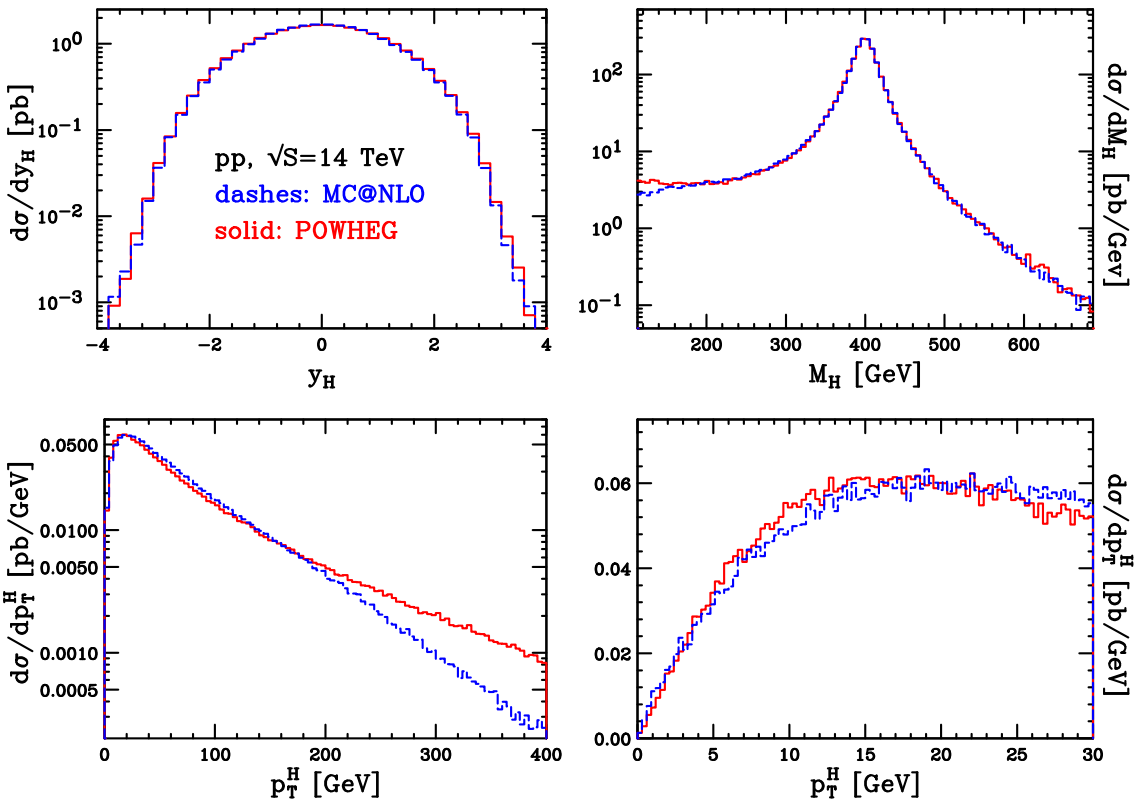

Figure 7. Comparison between POWHEG and MC@NLO for the rapidity, invariant mass and transverse-momentum distributions of a Higgs boson with $m_H = 400\,\text{GeV}$, at the LHC pp collider.

JHEP04(2009)002

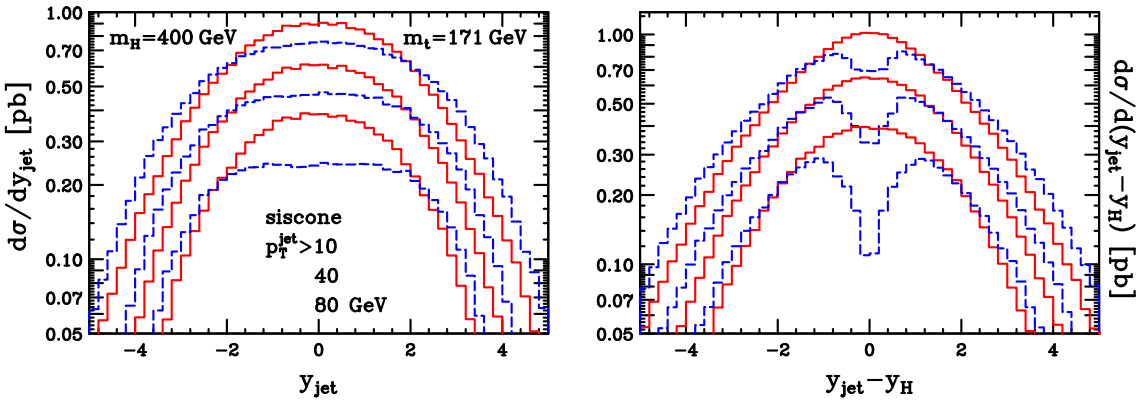

Figure 8. Comparison between POWHEG and MC@NLO for the rapidity of the leading jet and the rapidity difference of the Higgs boson and the leading jet, defined according to the SISCONE algorithm, with different jet cuts.

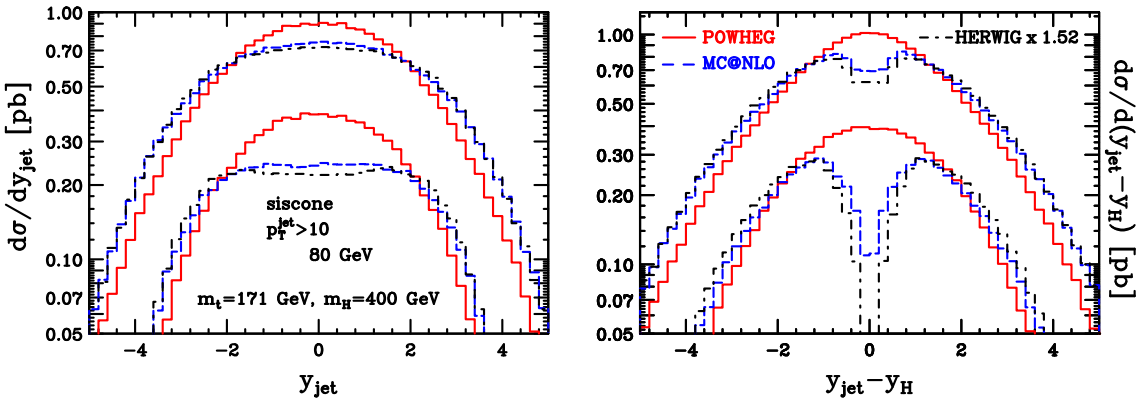

Figure 9. Comparison of POWHEG, MC@NLO and HERWIG (without matrix-element corrections), for the rapidity of the leading jet and the rapidity difference of the Higgs boson and the leading jet, defined according to the SISCONE algorithm, with different jet cuts.

JHEP04(2009)002

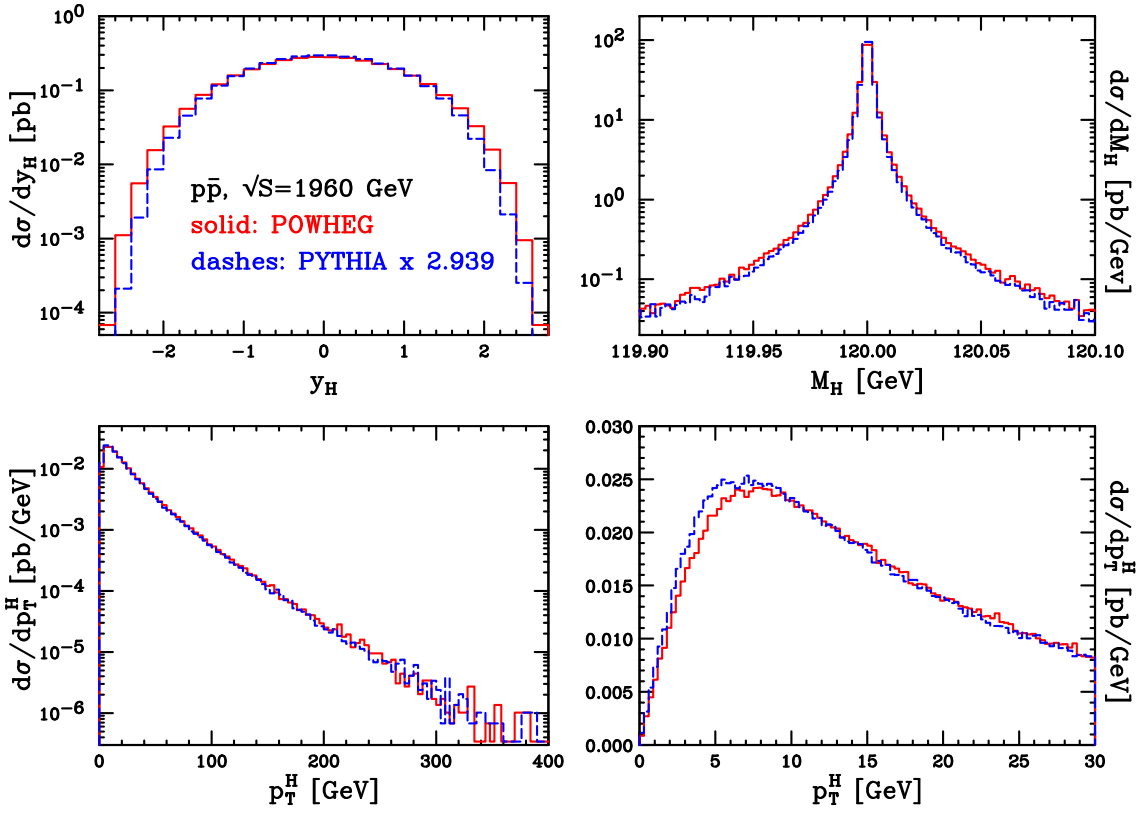

Figure 10. Comparison between POWHEG and PYTHIA for the rapidity, invariant mass and transverse-momentum distributions of a Higgs boson with $m_H = 120\,\text{GeV}$, at Tevatron $p\bar{p}$ collider. PYTHIA outputs normalized to the POWHEG cross section.

of the Higgs boson virtuality, distributed now according to

$$\frac{1}{\pi}\frac{M^2\,\Gamma_H/m_H}{\left(M^2-m_H^2\right)^2+\left(M^2\,\Gamma_H/m_H\right)^2}\,, \tag{4.2}$$

which is very similar to the form used in PYTHIA, except for the fact that PYTHIA includes threshold effects in the calculation of the Higgs boson width. In fact, PYTHIA uses a running $\Gamma_H(M^2)$, that increases when a decay channel opens up. The effects of using a fixed or a running Γ_H are more evident for a heavy Higgs boson, as will be shown in the following.

In figures 10 through 12 we compare results for the Tevatron $p\bar{p}$ collider, while in figures 13 through 15 we present results for the LHC. In all the plots we have set $m_H = 120\,\text{GeV}$. Results are in an impressive good agreement, both for inclusive quantities and for more exclusive ones. The only visible difference is in the transverse Higgs boson momentum distribution at low p_T at the LHC. This could be due to the different choice of the renormalization and factorization scale in the generation of radiation, our choice being constrained by the requirement of next-to-leading logarithmic accuracy in the Sudakov form factor.

JHEP04(2009)002

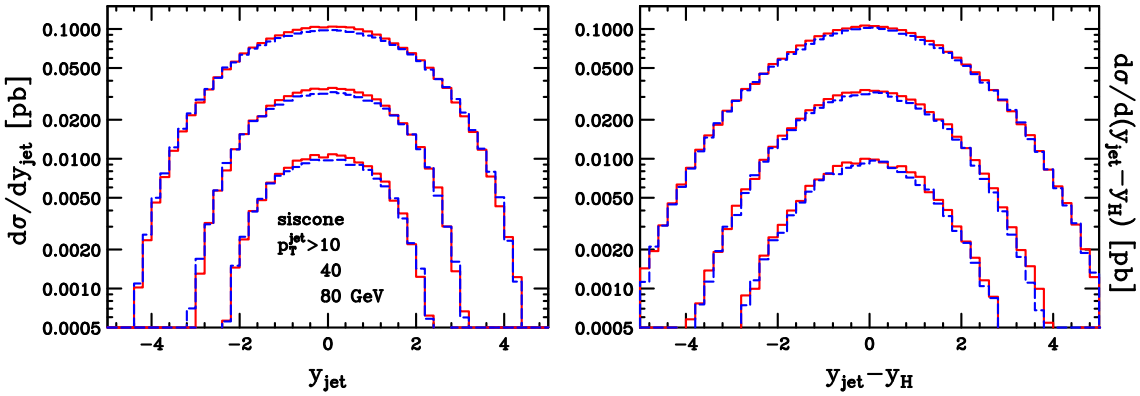

Figure 11. Comparison between POWHEG and PYTHIA for the rapidity of the leading jet and the rapidity difference of the Higgs boson and the leading jet, defined according to the SISCONE algorithm, with different jet cuts. PYTHIA outputs are normalized to the POWHEG cross section.

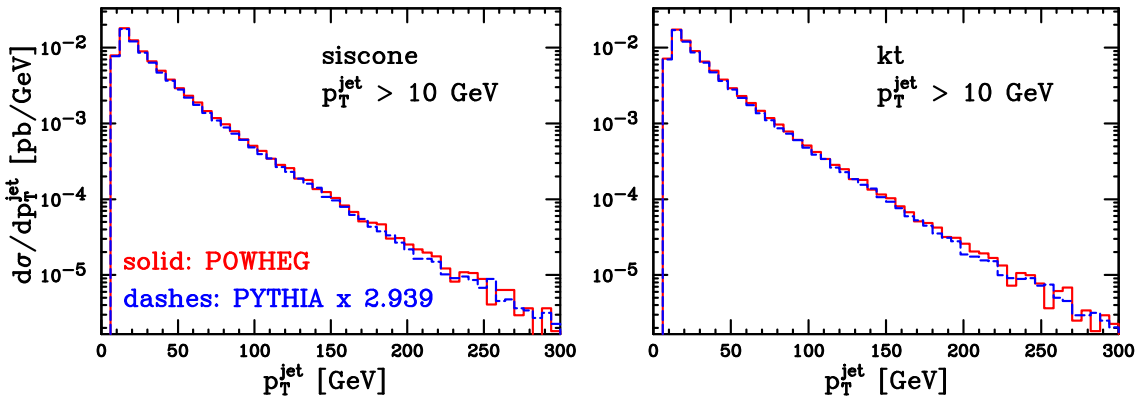

Figure 12. Comparison between POWHEG and PYTHIA for the transverse-momentum distributions of the leading jet, defined according to the SISCONE and the KT algorithms. PYTHIA outputs are normalized to the POWHEG cross section.

In figure 16 we present a comparison with $m_H = 400\,\text{GeV}$. Mass thresholds effects in Γ_H are evident in the invariant-mass distribution generated by PYTHIA. Below $2\,m_t$ the total width is smaller than the fixed one we are using, and PYTHIA results are accordingly lower than ours. All other plots show instead good agreement with POWHEG. The good agreement between POWHEG and PYTHIA was to some extent expected. As already observed in refs. [9, 14], the matrix-element correction method used in PYTHIA [27, 28] bears considerable similarities to POWHEG.

4.3 The p_T distribution in POWHEG

In this section we address the discrepancy in the p_T distributions in POWHEG and in MC@NLO. First of all, we show in figure 17 a comparison between the p_T spectrum of POWHEG, MC@NLO and the NLO calculation. For sake of comparison, we have used in POWHEG and in the NLO

JHEP04(2009)002

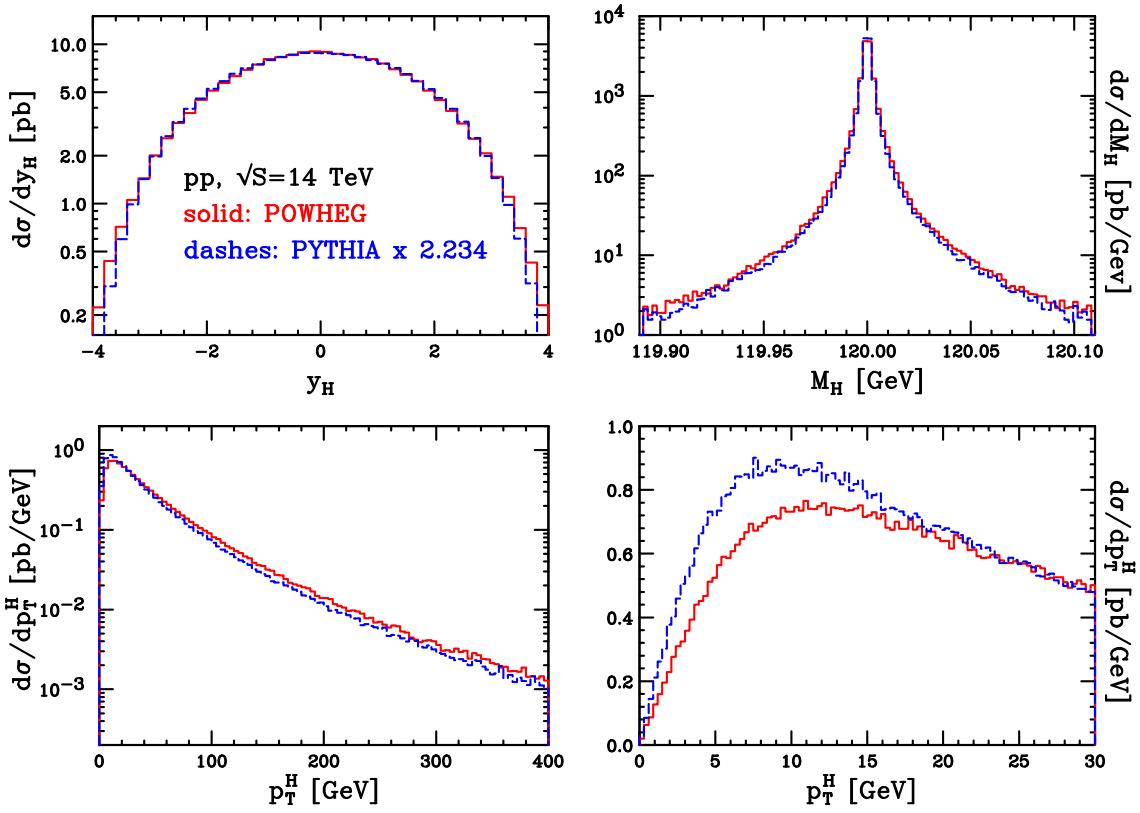

Figure 13. Comparison between POWHEG and PYTHIA for the rapidity, invariant mass and transverse-momentum distributions of a Higgs boson with $m_H = 120\,\text{GeV}$, at the LHC. PYTHIA outputs are normalized to the POWHEG cross section.

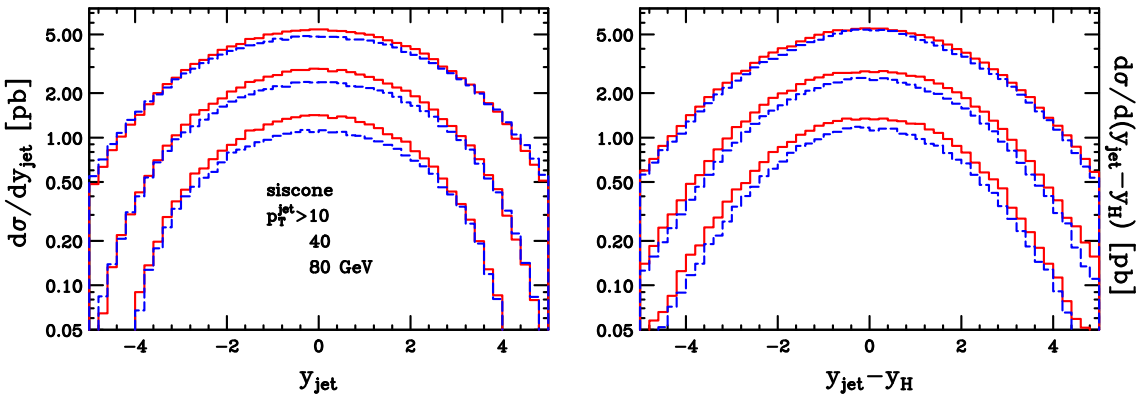

Figure 14. Comparison between POWHEG and PYTHIA for the rapidity of the leading jet and the rapidity difference of the Higgs boson and the leading jet, defined according to the SISCONE algorithm, with different jet cuts. PYTHIA outputs are normalized to the POWHEG cross section.

JHEP04(2009)002

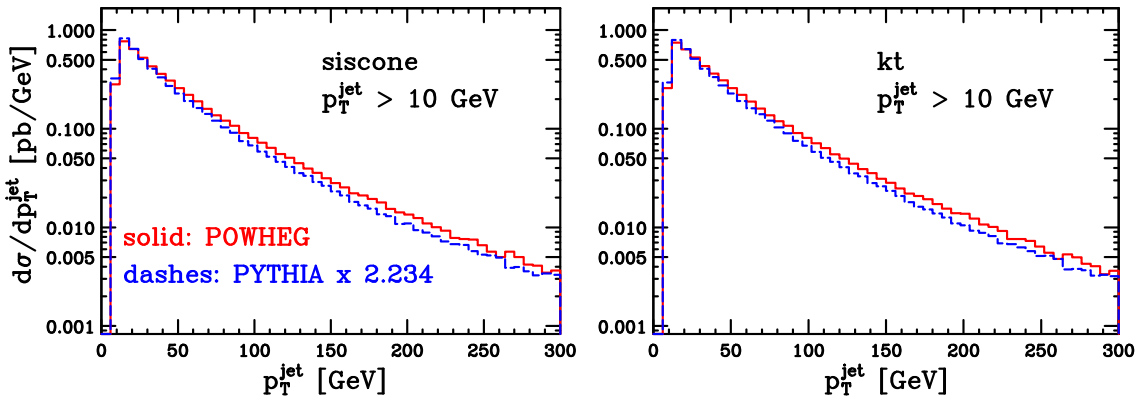

Figure 15. Comparison between POWHEG and PYTHIA for the transverse-momentum distributions of the leading jet, defined according to the SISCONE and the KT algorithms. PYTHIA outputs are normalized to the POWHEG cross section.

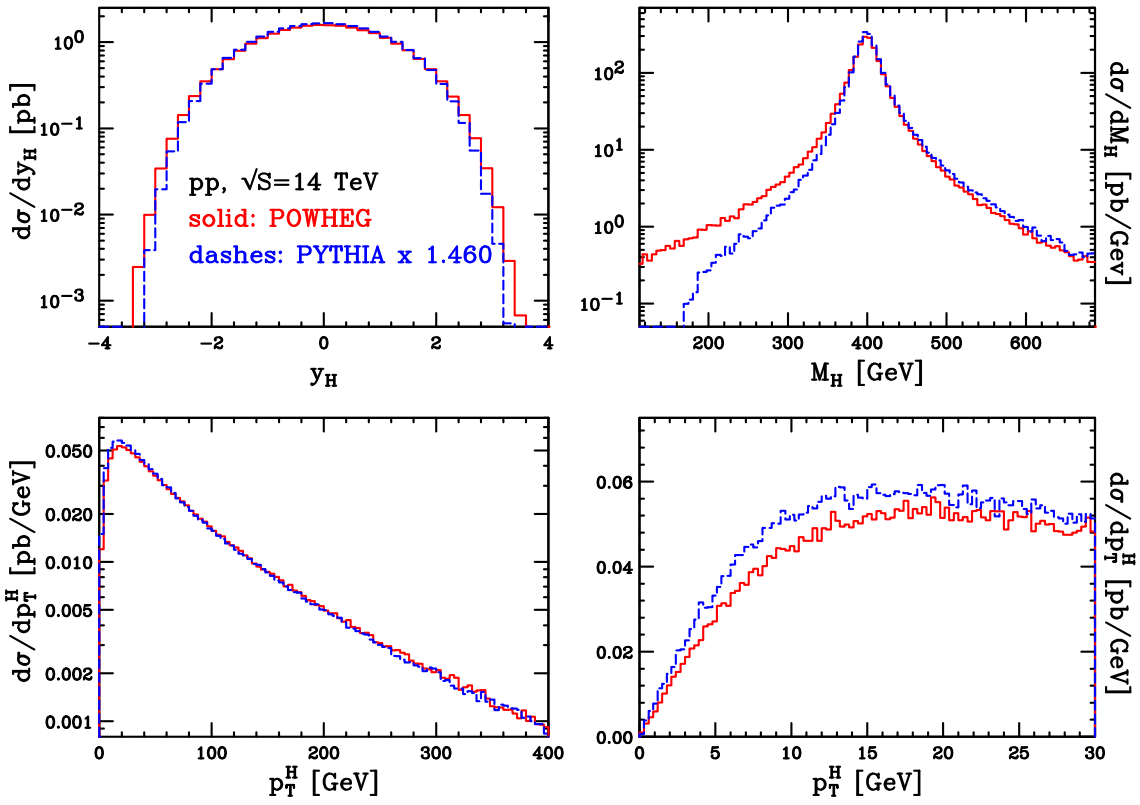

Figure 16. Comparison between POWHEG and PYTHIA for the rapidity, invariant mass and transverse-momentum distributions of a Higgs boson with $m_H = 400\,\text{GeV}$, at the LHC. PYTHIA outputs are normalized to the POWHEG cross section.

JHEP04(2009)002

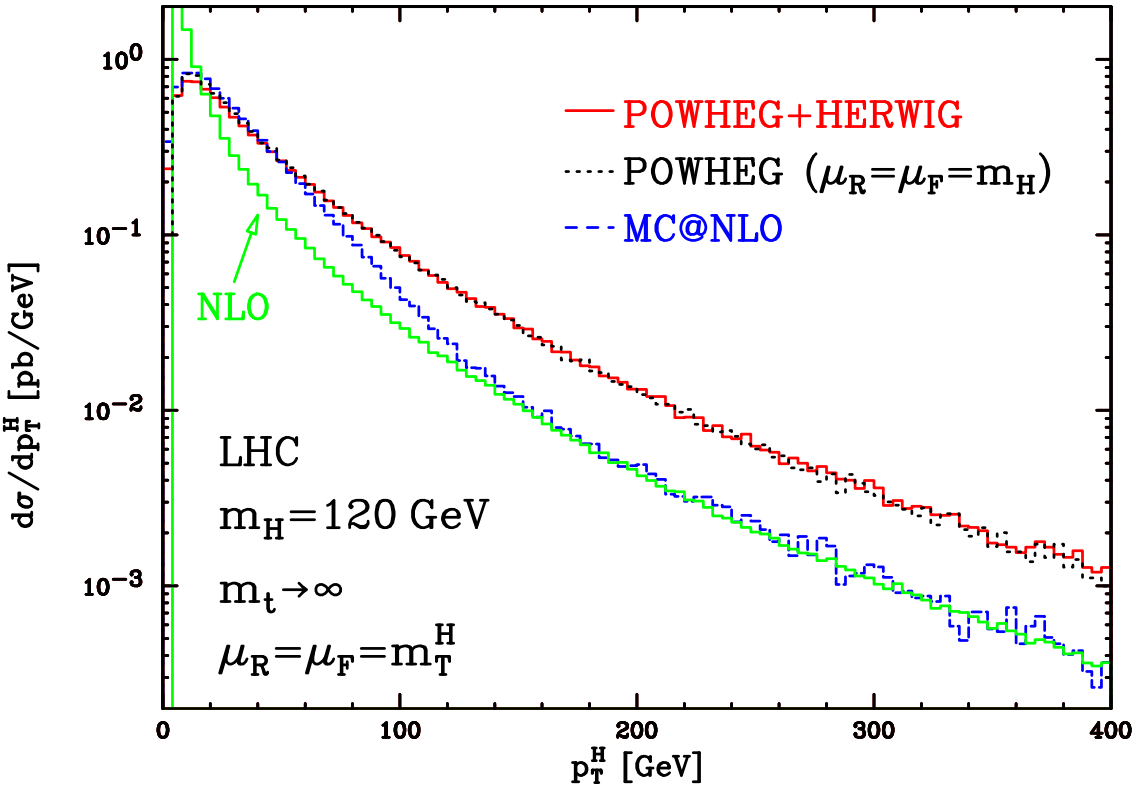

Figure 17. Comparison between POWHEG, MC@NLO and the NLO calculation, for $m_H = 120\,\text{GeV}$ at the LHC. All calculations are performed in the $m_t \to \infty$ approximation. Shower and hadronization are included in the MC results. The POWHEG result is also presented without shower and hadronization, and with a fixed-scale choice.

calculation the same scale choice adopted in MC@NLO. We point out, however, that using a scale that depends upon the transverse momentum of radiation in POWHEG can only affect the $\bar{B}$ function. More specifically, one ends up using a transverse momentum dependent scale only in calculation of the real contributions in $\bar{B}$, since the transverse momentum is zero for the Born, virtual and collinear remnant terms. Thus, this scale does not depend upon the transverse momentum of the real radiation, that is generated afterwards using the POWHEG Sudakov form factor. The choice of scale for radiation affects instead a single power of the coupling constant, since the Sudakov exponent is proportional to α_S. At low transverse momentum, this scale cannot be changed without spoiling the NLL accuracy of the Sudakov form factor. It can be changed, however, at large transverse momentum to explore further uncertainties. However, we have preferred not to implement this possibility. One should recall, in fact, that this scale only affects a single power of α_S, and it thus has a much smaller effect than a scale change in the NLO cross section.

We see from figure 17 that MC@NLO agrees better than POWHEG with the NLO calculation at large p_T. Since the difference between MC@NLO and POWHEG should be of next-to-next-to-leading order (NNLO), the difference between POWHEG and the NLO result should also be

JHEP04(2009)002

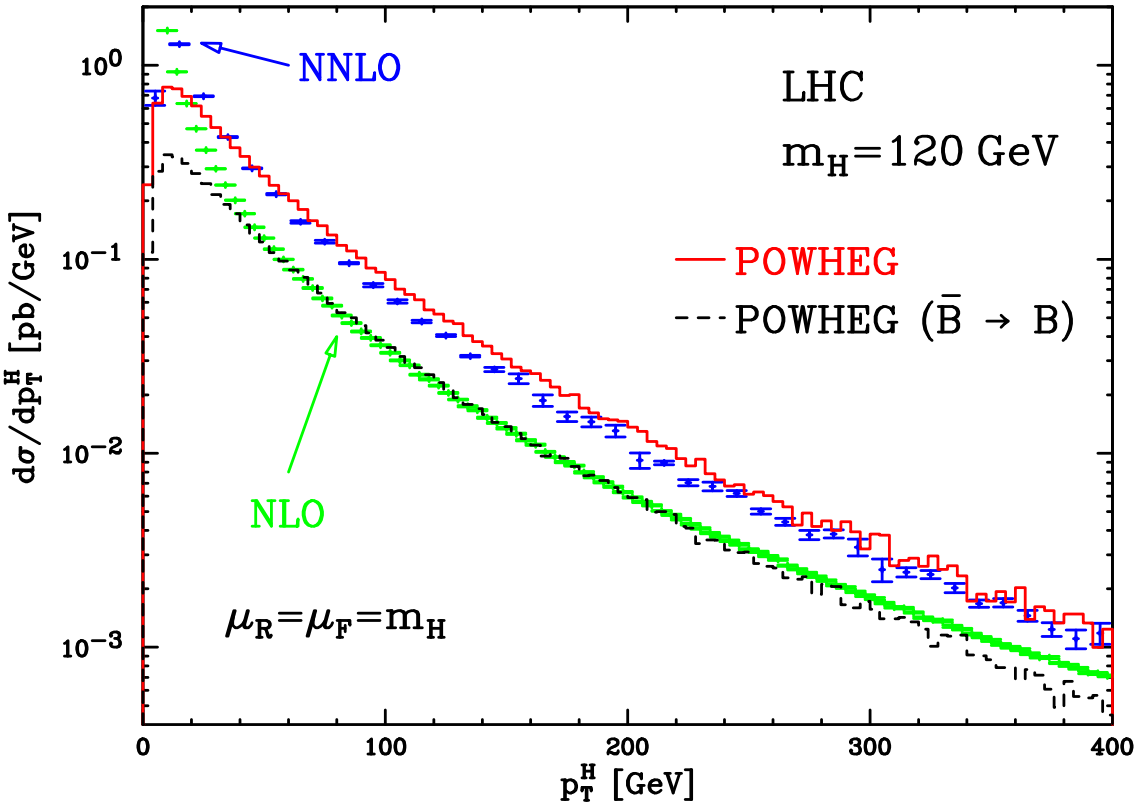

Figure 18. Comparison between POWHEG and fixed NLO and NNLO distributions for the transverse-momentum of the Higgs boson. Plots are done for $m_H = 120\,\text{GeV}$ at the LHC.

of NNLO. In fact we can easily trace the origin of this difference. From eq. (3.37), we infer that, at large p_T, the POWHEG differential cross section can be written as

$$d\sigma = \left[\bar{B}(\bar{\Phi}_1)\,\frac{R\left(\Phi_2\right)}{B\left(\bar{\Phi}_1\right)} + \sum_q R_{q\bar{q}}\left(\Phi_2\right)\right] d\bar{\Phi}_1\, d\Phi_{\text{rad}}\,, \tag{4.3}$$

since the Sudakov form factor approaches 1 in this region. Neglecting the subdominant $q\bar{q}$ real contribution, this differs from the pure NLO result because of the presence of the factor

$$\frac{\bar{B}(\bar{\Phi}_1)}{B\left(\bar{\Phi}_1\right)} = 1 + \mathcal{O}(\alpha_S)\,. \tag{4.4}$$

It is known that radiative corrections in Higgs boson production are large, so that the $\mathcal{O}(\alpha_S)$ term is in fact of order 1, and thus we find an enhancement that approaches a factor of two.[3] We have performed a clear cut test of this interpretation of the discrepancy. We have replaced the $\bar{B}$ function with the Born term B in the POWHEG program. The result of this calculation is shown in comparison with the NLO curve in figure 18. Since, as shown in

[3]We recall that normally the numerator and denominator in this factor are evaluated at different scales, since in $\bar{B}$ one uses a scale of the order of the Higgs boson transverse mass, while in the B term, one uses the transverse momentum. However, at large p_T, the two scales become of the same order.

JHEP04(2009)002

figure 17, the shower and hadronization are irrelevant for this distribution, we do not include them in the figure. In figure 18 we have chosen to use $p_{\rm T}$ independent renormalization and factorization scales, in order to perform a consistent comparison. Notice that, with this choice of scales, the NLO distribution is harder than the one shown in figure 17. This is easily explained by the fact that the NLO process is proportional to $\alpha_{\rm S}^3(\mu_{\rm R})$, and thus a $p_{\rm T}$ dependent renormalization scale can alter significantly the $p_{\rm T}$ distribution.

At this point, we can ask whether the higher order terms included in POWHEG with the mechanism illustrated above do in fact give a reasonable estimate of true NNLO effects. We thus include in figure 18 the NNLO result, obtained from the HNNLO program of ref. [16]. The result shows a rather good agreement between the NNLO result and POWHEG. Thus, our seemingly large corrections to the Higgs boson $p_{\rm T}$ distributions are in fact very similar in size to the full NNLO result. Observe that in figure 18 we have used a fixed scale choice for all the results. We were forced to do this, since the HNNLO program does not allow for other choices. However, because of the good agreement of the two POWHEG results in figure 17, and because of the smaller scale dependence of the NNLO result, this should not make a severe difference.

Because of a fortuitous circumstance, we did not need to worry about correcting for the large difference between the POWHEG and the NLO result at large radiation transverse momentum, since the known NNLO result seems to support the POWHEG one. We remark, however, that, had this not been the case, it is very easy to modify the POWHEG algorithm so to obtain a $p_{\rm T}$ spectrum that agrees with the NLO calculation at large $p_{\rm T}$. This can be done as follows. Instead of using the full real cross section for the computation of the $\bar{B}$ function and of the Sudakov form factor, we can instead use a reduced real contribution

$$R^{\rm red} = R \times F\,, \tag{4.5}$$

where F is a function of the real phase space, with $F < 1$ everywhere, such that F approaches 1 for small transverse momenta, and approaches zero for large transverse momenta. We perform the POWHEG generation using $R^{\rm red}$ instead of R, and treat the remaining $R \times (1-F)$ contribution to the cross section with the same method that we used for the $R_{q\bar{q}}$ contribution. This can be done, since $R \times (1-F)$ is dumped by the $1-F$ factor in the singular region. It will then follow that, for large transverse momentum, the result would agree with the NLO calculation, since it would be dominated by the $R \times (1-F)$ contribution. It turned out that, in all previous implementations, it was not necessary to use such procedure. As remarked before, thanks to the known properties of the NNLO result, this was not necessary even in this case. We have however performed such study, just in order to illustrate the flexibility of the POWHEG method. We have chosen for F the following form

$$F = \frac{h^2}{p_{\rm T}^2 + h^2}\,. \tag{4.6}$$

The resulting transverse-momentum distribution at the LHC, for a Higgs boson mass of 400 GeV, is shown in figure 19 for $h \to \infty$ (standard POWHEG), $h = 120\,\text{GeV}$ and $h = 400\,\text{GeV}$. One can see that it is not difficult to get distributions that undershoot the MC@NLO one in the intermediate range of $p_{\rm T}$. We also observe that, with this procedure, no undesired

JHEP04(2009)002

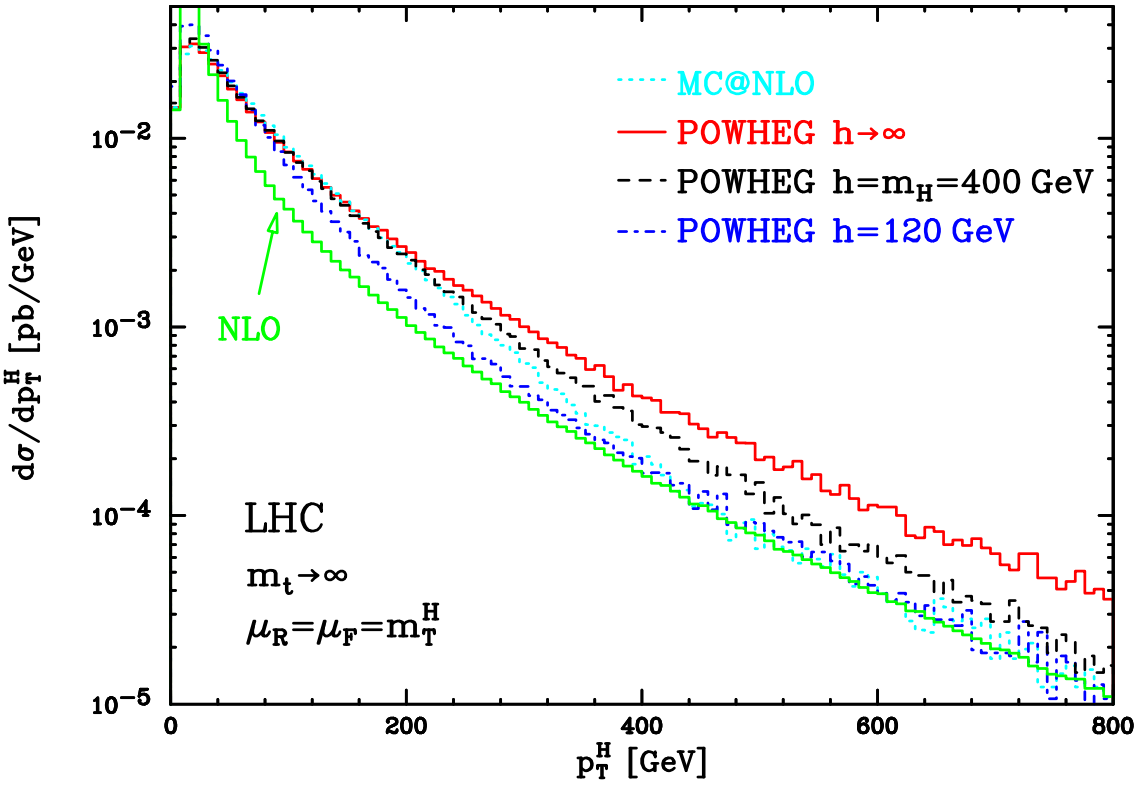

Figure 19. Comparison of the predictions of MC@NLO, standard POWHEG ($h \to \infty$) and POWHEG with two different values of the parameter h ($h = 120\,\text{GeV}$ and $h = m_H = 400\,\text{GeV}$) in the function F of eq. (4.6), for the transverse-momentum distributions of a Higgs boson, at the LHC pp collider.

features of other distributions appear. In particular, the distribution in the rapidity of the hardest jet, and in the rapidity difference between the hardest jet and the Higgs boson remain qualitatively the same, as shown in figure 20.

4.4 Next-to-leading logarithmic resummation

As explained in section (4.4) of ref. [9], one can reach next-to-leading logarithmic (NLL) accuracy of soft gluon resummation if the number of coloured partons involved in the hard scattering is less or equal to three. This can be obtained by replacing the strong coupling constant in the Sudakov exponent with [29]

$$\alpha_{\text{S}} \to A\left(\alpha_{\text{S}}\left(k_{\text{T}}^2\right)\right), \qquad A(\alpha_{\text{S}}) = \alpha_{\text{S}}\left\{1 + \frac{\alpha_{\text{S}}}{2\pi}\left[\left(\frac{67}{18} - \frac{\pi^2}{6}\right)C_{\text{A}} - \frac{5}{9}n_{\text{f}}\right]\right\}, \tag{4.7}$$

where the $\overline{\text{MS}}$, 1-loop expression of α_{S} should be used. The previous replacement may also be implemented by a simple redefinition of the strong scale Λ, which, for five active flavours ($n_{\text{f}} = 5$), becomes $\Lambda_{\text{MC}} \equiv 1.569\,\Lambda^{(5)}_{\overline{\text{MS}}}$. We have exploited this possibility in our code, so that our result should agree with the NLL resummed one. A comparison has been thus carried out with the HqT [30] program, that performs such a resummation. We have

JHEP04(2009)002

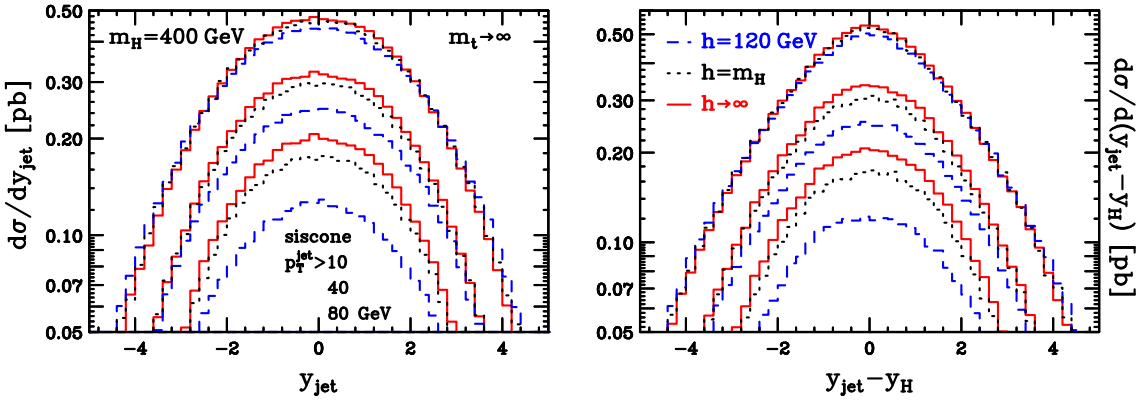

Figure 20. Comparison of the predictions of the standard POWHEG ($h \to \infty$), and POWHEG with two different values of the parameter h ($h = 120\,\text{GeV}$ and $h = m_H = 400\,\text{GeV}$) in the function F of eq. (4.6), for the rapidity of the leading jet and the rapidity difference of the Higgs boson and the leading jet, defined according to the SISCONE algorithm, with different jet cuts, at the LHC.

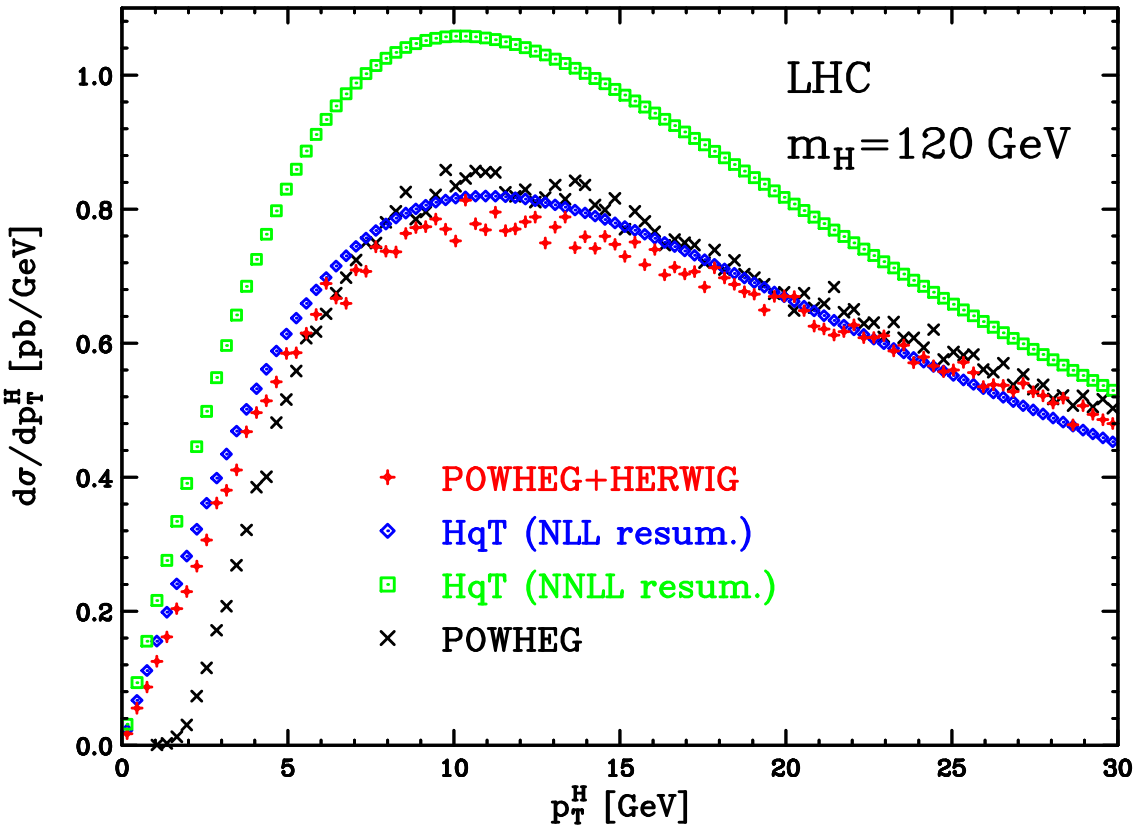

Figure 21. Comparison between POWHEG and HqT for the transverse-momentum distributions of a Higgs boson, at the LHC. The POWHEG result without shower and hadronization is also shown.

JHEP04(2009)002

adopted fixed renormalization and factorization scales. Results are shown in figure 21, together with next-to-next-to-leading logarithmic (NNLL) resummation, always from HqT, just for reference purposes. We see a fair agreement between the POWHEG result and the NLL analytic one, as expected. The different behaviour of the POWHEG result without shower and hadronization at very low $p_{\rm T}$ may be ascribed to the particular implementation of the minimum transverse momentum that we use, that is, to a large extent, arbitrary.

We observe that, in all cases, we do not expect full agreement between the POWHEG result without shower, and the NLL calculation. In fact, the POWHEG curve without shower represents the Sudakov form factor for the $p_{\rm T}$ of the hardest emission, while, in the NLL calculation, the total $p_{\rm T}$ distribution (i.e. the sum of the transverse momenta of all emissions) is considered. Thus, it is only after the inclusion of the full shower effects that the two distributions have a meaningful comparison.

5 Conclusions

In this paper we have reported on a complete implementation of Higgs boson production via gluon fusion at next-to-leading order in QCD, in the POWHEG framework. The calculation was performed within the Frixione-Kunszt-Signer [20, 21] subtraction approach. We have also shown how to deal with non-singular real contributions, that do not present a valid underlying Born matrix element.

The results of our work have been compared extensively with MC@NLO and PYTHIA shower Monte Carlo programs. The PYTHIA results, normalized to the total NLO cross section, are in good agreement with POWHEG, except for differences in the low transverse-momentum distributions of the Higgs boson at the LHC. The MC@NLO results are in fair agreement with POWHEG, except for the $p_{\rm T}$ distribution of the Higgs boson, and consequently of the hardest jet, in the high-$p_{\rm T}$ region. In this region the POWHEG distributions are generally harder. We have shown that this is due to NNLO effects in the POWHEG formula for the differential cross section. We checked that these effects actually bring our result closer to the NNLO one [16]. The low-$p_{\rm T}$ region was instead tested against the analytic resummed results [30]. We find again good agreement up to NLL accuracy.

Furthermore, we have also examined the distributions in the difference of the hardest jet and the Higgs boson rapidity. The dip found in previous implementations [10, 11, 14] is still present. We remark that this seems to be a general feature of MC@NLO, since other calculations do not find effects of this kind [17–19].

The computer code for the POWHEG implementations presented in this paper is available, together with the manual, at the site

http://moby.mib.infn.it/~nason/POWHEG

References

[1] S. Dawson, *Radiative corrections to Higgs boson production*, *Nucl. Phys.* **B 359** (1991) 283 [SPIRES].

[2] A. Djouadi, M. Spira and P.M. Zerwas, *Production of Higgs bosons in proton colliders: qCD corrections*, *Phys. Lett.* **B 264** (1991) 440 [SPIRES].

JHEP04(2009)002

[3] M. Spira, A. Djouadi, D. Graudenz and P.M. Zerwas, *Higgs boson production at the LHC*, *Nucl. Phys.* **B 453** (1995) 17 [hep-ph/9504378] [SPIRES].

[4] S. Frixione and B.R. Webber, *Matching NLO QCD computations and parton shower simulations*, *JHEP* **06** (2002) 029 [hep-ph/0204244] [SPIRES].

[5] G. Corcella et al., *HERWIG 6.5: an event generator for Hadron Emission Reactions With Interfering Gluons (including supersymmetric processes)*, *JHEP* **01** (2001) 010 [hep-ph/0011363] [SPIRES].

[6] G. Corcella et al., *HERWIG 6.5 release note*, hep-ph/0210213 [SPIRES].

[7] T. Sjöstrand, S. Mrenna and P. Skands, *PYTHIA 6.4 Physics and Manual*, *JHEP* **05** (2006) 026 [hep-ph/0603175] [SPIRES].

[8] P. Nason, *A new method for combining NLO QCD with shower Monte Carlo algorithms*, *JHEP* **11** (2004) 040 [hep-ph/0409146] [SPIRES].

[9] S. Frixione, P. Nason and C. Oleari, *Matching NLO QCD computations with parton shower simulations: the POWHEG method*, *JHEP* **11** (2007) 070 [arXiv:0709.2092] [SPIRES].

[10] P. Nason and G. Ridolfi, *A positive-weight next-to-leading-order Monte Carlo for Z pair hadroproduction*, *JHEP* **08** (2006) 077 [hep-ph/0606275] [SPIRES].

[11] S. Frixione, P. Nason and G. Ridolfi, *A positive-weight next-to-leading-order Monte Carlo for heavy flavour hadroproduction*, *JHEP* **09** (2007) 126 [arXiv:0707.3088] [SPIRES].

[12] O. Latunde-Dada, S. Gieseke and B. Webber, *A positive-weight next-to-leading-order Monte Carlo for e^+e^- annihilation to hadrons*, *JHEP* **02** (2007) 051 [hep-ph/0612281] [SPIRES].

[13] O. Latunde-Dada, *Applying the POWHEG method to top pair production and decays at the ILC*, *Eur. Phys. J.* **C 58** (2008) 543 [arXiv:0806.4560] [SPIRES].

[14] S. Alioli, P. Nason, C. Oleari and E. Re, *NLO vector-boson production matched with shower in POWHEG*, *JHEP* **07** (2008) 060 [arXiv:0805.4802] [SPIRES].

[15] K. Hamilton, P. Richardson and J. Tully, *A positive-weight next-to-leading order Monte Carlo simulation of Drell-Yan vector boson production*, *JHEP* **10** (2008) 015 [arXiv:0806.0290] [SPIRES].

[16] S. Catani and M. Grazzini, *An NNLO subtraction formalism in hadron collisions and its application to Higgs boson production at the LHC*, *Phys. Rev. Lett.* **98** (2007) 222002 [hep-ph/0703012] [SPIRES].

[17] M.L. Mangano, M. Moretti, F. Piccinini and M. Treccani, *Matching matrix elements and shower evolution for top- quark production in hadronic collisions*, *JHEP* **01** (2007) 013 [hep-ph/0611129] [SPIRES].

[18] J. Alwall et al., *Comparative study of various algorithms for the merging of parton showers and matrix elements in hadronic collisions*, *Eur. Phys. J.* **C 53** (2008) 473 [arXiv:0706.2569] [SPIRES].

[19] S. Dittmaier, P. Uwer and S. Weinzierl, *Hadronic top-quark pair production in association with a hard jet at next-to-leading order QCD: phenomenological studies for the Tevatron and the LHC*, *Eur. Phys. J.* **C 59** (2009) 625 [arXiv:0810.0452] [SPIRES].

[20] S. Frixione, Z. Kunszt and A. Signer, *Three jet cross-sections to next-to-leading order*, *Nucl. Phys.* **B 467** (1996) 399 [hep-ph/9512328] [SPIRES].

JHEP04(2009)002

[21] S. Frixione, *A general approach to jet cross-sections in QCD*, *Nucl. Phys.* **B 507** (1997) 295 [hep-ph/9706545] [SPIRES].

[22] P. Nason, *MINT: a computer program for adaptive Monte Carlo integration and generation of unweighted distributions*, arXiv:0709.2085 [SPIRES].

[23] P. Nason and G. Ridolfi, *A positive-weight next-to-leading-order Monte Carlo for Z pair hadroproduction*, *JHEP* **08** (2006) 077 [hep-ph/0606275] [SPIRES].

[24] J. Pumplin et al., *New generation of parton distributions with uncertainties from global QCD analysis*, *JHEP* **07** (2002) 012 [hep-ph/0201195] [SPIRES].

[25] G.P. Salam and G. Soyez, *A practical seedless infrared-safe cone jet algorithm*, *JHEP* **05** (2007) 086 [arXiv:0704.0292] [SPIRES].

[26] M. Cacciari and G.P. Salam, *Dispelling the N^3 myth for the k_t jet-finder*, *Phys. Lett.* **B 641** (2006) 57 [hep-ph/0512210] [SPIRES].

[27] M. Bengtsson and T. Sjöstrand, *Coherent parton showers versus matrix elements: implications of PETRA - PEP Data*, *Phys. Lett.* **B 185** (1987) 435 [SPIRES].

[28] T. Sjöstrand, *Monte Carlo Generators*, hep-ph/0611247 [SPIRES].

[29] S. Catani, B.R. Webber and G. Marchesini, *QCD coherent branching and semiinclusive processes at large x*, *Nucl. Phys.* **B 349** (1991) 635 [SPIRES].

[30] G. Bozzi, S. Catani, D. de Florian and M. Grazzini, *Transverse-momentum resummation and the spectrum of the Higgs boson at the LHC*, *Nucl. Phys.* **B 737** (2006) 73 [hep-ph/0508068] [SPIRES].

JHEP04(2009)002